Performance evaluation of sensor equipped tool holder

Johan Östholm
elt13jos@student.lu.se

Department of Electrical and Information Technology
Lund University

Supervisors:
Mikael Swartling, EIT
Anders Liljerehn, AB Sandvik Coromant
Peter Eriksson, AB Sandvik Coromant
Per-Olov Gustavsson, AB Sandvik Coromant

Examiner: Nedelko Grbic

June 9, 2018

Printed in Sweden
Tryckeriet i E-huset, Lund

Abstract

As Industry 4.0 becomes a reality in manufacturing, the need of accessing data from machining processes increases. In this thesis two tool holders with sensors equipped on them are evaluated and recommendations for future sensor equipped tool holders are presented. The sensors are designed to provide the user with information regarding bending moment and torque variation during machining in metal materials. The two tool holders were evaluated against a numerical force model and an external dynamometer as reference. An analysis of how having sensors mounted on the tool holders affects their stability and sensitivity to regenerative vibrations was also performed. Filters for reducing measurement distortion due to equipment dynamic characteristics are also obtained, hereby increasing the frequency range of the measurements. This was successfully implemented for the external dynamometer, however due to the sampling frequency of the sensor equipped tool holder such a filter could not be obtained.

This thesis was carried out at AB Sandvik Coromant.

Acknowledgements

First I would like to thank everyone at CDPVV at AB Sandvik Coromant for giving me the opportunity to conduct my master thesis there and utilize their facilities. Especially I would like to express my sincerest gratitude to my supervisors PhD. Anders Liljerehn, Per-Olov Gustansson, and Peter Eriksson for their invaluable support and showing great interest in my work and finally to my supervisor at EIT, PhD. Mikael Swartling for his guidance and help.

Table of Contents

Chapter 1
Introduction

1.1 Background

In order to shape and process metal materials CNC-machines are commomly used. Three very common processes used to shape material are milling, drilling and turning. During these processes both the workpiece material and the cutting tool are subjected to cutting forces. The ability to measure these forces accurate is of great importance in order to analyse the cutting process efficiency and estimate power, torque requirements.

One way of measuring these forces is to use external piezoelectric dynamometers mounted on the workpiece or on the tool. However, as machine integration becomes more and more important for the metal cutting industry, the need for these kind of sensors integrated within the machine tool increases. Having these kind of sensors integrated in the machine tool would expand the possibility of getting useful data from the cutting process. This data can be used as feedback directly to the machine tool or to the machine operator. Using the data in a smart way can help prevent unexpected cutting process failures [1]. The measured cutting forces have also be used as an input to a neural net to predict tool life in milling [2].

The first method for using integrated strain gauges to measure cutting force was presented by M. Santochi *et al.* in [3], which was achieved by mounting strain gauges close to the insert on a machine lathe. A wireless sensor integrated for measuring torque during end-milling operation was presented in [4] and different methods to measure cutting forces was researched in [5] and [6].

1.2 Aim and objective

The aim of this thesis is to evaluate and analyse if a sensor equipped tool holder performs with such accuracy that it can be of assistance in cutting process evaluation and cutting tool design. To determine this the objective is to compare two

sensor equipped tool holders, with a theoretical model, an external multi component dynamometer and an external rotating multi component dynamometer. The impact on the tool holders dynamic behaviour due to mounting of a sensor system is to be investigated to determine its impact on the tool holders stiffness. Further this investigation seeks to find an appropriate filtering technique to further enhance the quality of the measured data.

1.2.1 Research question

1. How does the sensor equipped tool holders perform compared to theoretical and established measurements systems in terms of amplitude, noise and shape of milling and drilling cutting forces
2. Will the mounting of the sensor system affect the tool holders dynamic behaviour and accessibility during cutting operations
3. How should a filter be designed to ensure minimal distortion of cutting force measurements due to dynamic influence

1.2.2 Limitations

To keep the project within the scope and timeframe, some limitations have been made.

- No study of thermal or spindle speed related measurement drift has been conducted
- The experimental milling and drilling tests were limited to only one cutting speed
- All experimental milling tests has been conducted using only one insert
- A filter for reducing dynamic influence has only been obtained for one experimental setup
- The filter for reducing dynamic influence were not adapted for zero phase filtering

1.3 Thesis outline

- **Chapter 1:** Introduction to the thesis and objectives.
- **Chapter 2:** Describes the theory needed to make the desired evaluation.
- **Chapter 3:** Methods of performed measurements and implementations.
- **Chapter 4:** Results of performed measurements and implementations.
- **Chapter 5:** Result evaluation.
- **Chapter 6:** Discussion and future work.

Chapter 2
Theory

This section contains the theoretical foundations of measurement and modelling of cutting forces in metal machining. This provides knowledge of how these models are obtained and how the different ways of measuring cutting forces work facilitates the evaluation. In order to understand how the mounting of a sensor system impacts the dynamic behaviour of tool holders and thereby affects which cutting parameters that may be used without causing an unstable cutting process, a mathematical connection between dynamic behaviour and its stability during machining is provided. Concerning the inverse filter obtained and investigated in this thesis, the theory behind it, its limitations and possibilities is required if such a filter is to be obtained and implemented correctly for cutting force measurements.

2.1 Modelling of cutting forces

This section introduces the basic equations and theory that are used throughout this thesis to perform the cutting force simulations. Most of the information in this section has been obtained from [7]. An important note regarding the theoretical calculations of cutting forces throughout this thesis is that the material dependent cutting force constants, for example k_{q1} in equation 2.1, were obtained through lathe tests, not milling tests.

The cutting force model used in this thesis is known as the Kienzle-model [8], which distinguishing it self by having an exponential dependence between the chip thickness and the specific cutting force. This is opposed to the model used in [7], which is a linear model. The Kienzle model, which is the most commonly used at AB Sandvik Coromant, is formulated as

$$F_q = k_{q1} \cdot h^{1-m_q} \cdot a_{\mathrm{p}} \cdot (1 - \frac{\gamma}{\gamma_{\mathrm{corr,q}}}) \tag{2.1}$$

where h is the uncut chip thickness, a_{p} is the depth of cut, γ is the rake angle, γ_{corr} is the correction factor of the rake angle, and k_{q1} and m_q are material dependent constants, which are obtained through experimental test data. Dividing this into axial segments, the contribution from each segment in q-direction is formulated as

$$dF_q = k_{q1} \cdot \Delta a_\mathrm{p} \cdot h_{pjr}^{1-m_q} \cdot (1 - \frac{\gamma}{\gamma_{\mathrm{corr,q}}}) \tag{2.2}$$

here k represents cutting tooth, j is the segment along the direction of depth of cut a_p, and p is the segment in angular rotation of the tool. This is visualised in figures 2.1 and 2.2. The force contribution from each segment, dF_q, is dependent on which angular position, ϕ_{pjr}, the segment has. This since h_{pjr} is dependent on the segments angular position as

$$h_{pjr} = f_z \cdot \sin(\phi_{pjr}) \tag{2.3}$$

Here it should be noted that due to λ_s the angular position of each segment, ϕ_{pjr}, will be dependent on its axial position, j, and on which tooth that the segment is acting. Thereby ϕ_{pjr} might be different from the cutting tool angular position, ϕ_p. The dependence is as

$$\phi_{pjr} = \phi_{ci} + p \cdot \Delta\phi + (r-1)\phi_{pitch} - \frac{2\tan(\lambda_s)}{D_\mathrm{cap}} \cdot j \cdot \Delta a_\mathrm{p} \tag{2.4}$$

where ϕ_pitch is the angle between each cutting tooth and $\Delta\phi$ is the angular difference between each angle segment, ϕ_p. During a milling process, the total force is divided into 3 components: tangential, radial and axial force. Which each contribute to the total force acting on the workpiece. Using equation 2.2 and summing over all r, and j the contribution from each of these forces for each angle of the tool, ϕ_p, is expressed as

$$F_t(\phi_p) = \sum_{r=1}^{z}\sum_{j=0}^{L} dF_t(\phi_{pjr}) \quad F_r(\phi_p) = \sum_{r=1}^{z}\sum_{j=0}^{L} dF_r(\phi_{pjr}) \quad F_a(\phi_p) = \sum_{r=1}^{z}\sum_{j=0}^{L} dF_a(\phi_{pjr}) \tag{2.5}$$

where $\phi_{ci} < \phi_{ijk} < \phi_{co}$, ϕ_{ci} and ϕ_{co} are the angular span between which the tooth enters and exits cutting, and z is the number of teeth. If a tooth is outside this region its contribution to the respective force is 0.

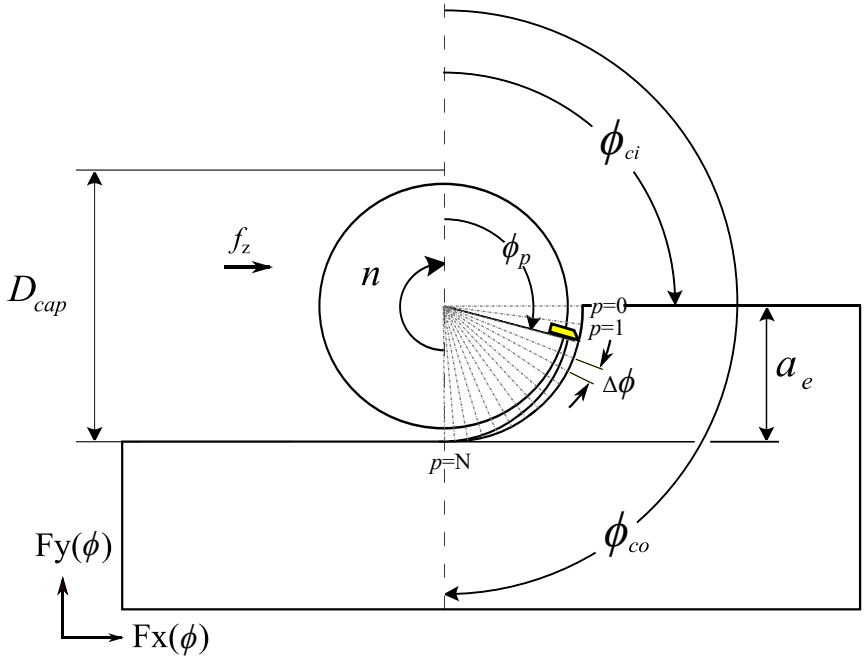

Figure 2.1: Top view of milling engagement with visualisation of notations

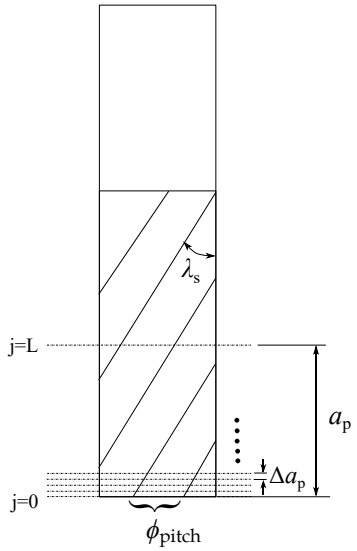

Figure 2.2: Side view of mill with visualisation of notations

Calculating the sums in equation 2.5 for each ϕ_p gives an estimation of how the cutting forces varies throughout a cutting engagement. Figure 2.3 shows an ex-

ample of a milling operation simulated with the method described above, using cutting force coefficients derived from for workpiece material 34CrNiMo56.

As the reference measurements with the multi component force dynamometer is performed in stationary Cartesian coordinates while the sensor equipped tool hoders measures in a rotating coordinate system, a transformation is needed. This transformation to a stationary coordinate system, F_x and F_y, is calculated as

$$\begin{bmatrix} F_x(\phi(t)) \\ F_y(\phi(t)) \end{bmatrix} = \begin{bmatrix} -\cos(\phi(t)) & -\sin(\phi(t)) \\ \sin(\phi(t)) & -\cos(\phi(t)) \end{bmatrix} \begin{bmatrix} F_t(\phi(t)) \\ F_r(\phi(t)) \end{bmatrix} \tag{2.6}$$

The force acting in the axial direction, F_a, was not considered in the milling evaluation.

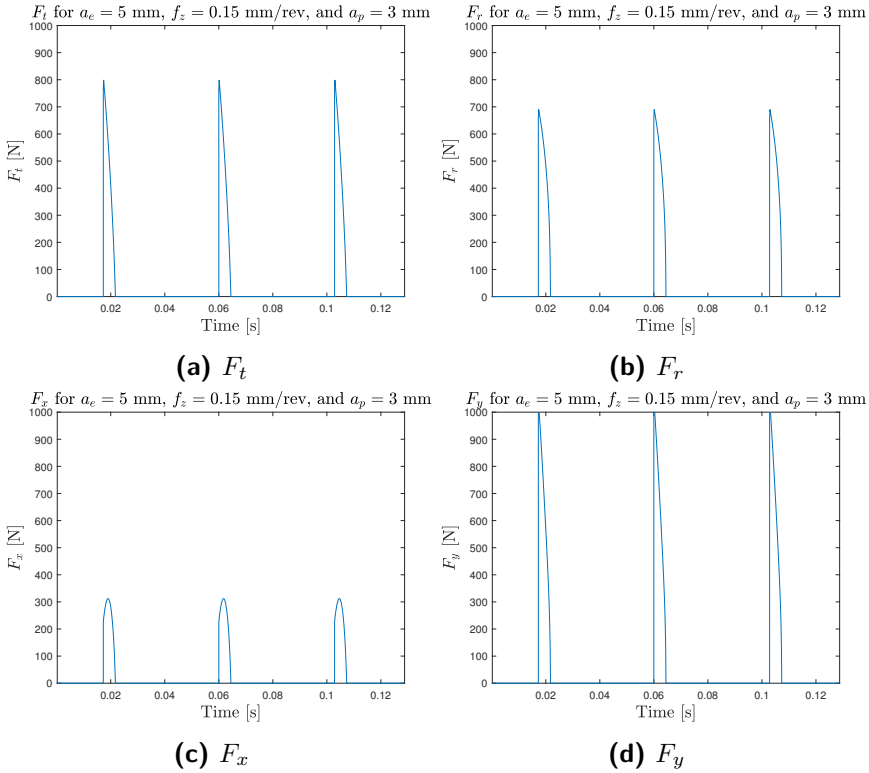

(a) F_t **(b)** F_r

(c) F_x **(d)** F_y

Figure 2.3: Shows example of F_t, F_r, F_x, and F_y for a single tooth, $z = 1$, milling operation with $a_e = 5\,\mathrm{mm}$, $f_z = 0.15\,\mathrm{mm}$, $a_\mathrm{p} = 3\,\mathrm{mm}$, $\gamma = -20$, $\gamma_{\mathrm{corr,t}} = 100$, and $\gamma_{\mathrm{corr,r}} = 40$ simulated for 3 revolutions

2.2 Tool holder stability

Given the input force signal, $x_F(t)$, and the output acceleration, $x_a(t)$, the coherence between these is calculated as

$$C_{xy}(f) = \frac{|P_{x_a x_F}(f)|^2}{P_{x_a x_a}(f) P_{x_F x_F}(f)} \tag{2.7}$$

where $P_{x_a x_a}(f)$ and $P_{x_F x_F}(f)$ are the power spectral densities and $P_{x_a x_F}(f)$ is the cross power spectral density, of the time sequences $x_F(t)$ and $x_a(t)$. This is ideally equal to 1 for all frequencies, which would indicate a linear relationship between $x_F(t)$ and $x_a(t)$. However, in this thesis this was used to determine if the measurement of accelerance FRF, $H_a(\omega)$, was good enough, or if it had be performed once again. The measured FRFs and their corresponding coherence can be seen in appendix A. The FRF, $H_a(\omega)$, is obtained by using the frequency domain representation of the signals, $x_F(t)$ and $x_a(t)$ as

$$H_a(\omega) = \frac{X_a(\omega)}{X_F(\omega)} \tag{2.8}$$

The FRFs for velocity and displacement is obtained by integrating $H_a(\omega)$ in frequency domain according to

$$H_v(\omega) = \frac{H_a(\omega)}{i\omega} \tag{2.9}$$

and

$$H_d(\omega) = \frac{H_v(\omega)}{i\omega} \tag{2.10}$$

Having the FRF in displacement, $H_d(\omega)$, is needed for calculations of the chatter stability lobes and the critical depth of cut, $a_{\mathrm{p}}^{\mathrm{lim}}$; which is the maximum depth of cut for which the cutting process is stable for all spindle speeds. The relationship between these is seen in figure 2.4. Using the theory on chatter vibrations described in [9], [10] and [11], the relationship between acquired H_d and $a_{\mathrm{p}}^{\mathrm{lim}}$ is as

$$a_{\mathrm{p}}^{\mathrm{lim}} = -\frac{2\pi \Im\{\lambda\}}{N k_t}(\kappa + \frac{1}{\kappa}) \tag{2.11}$$

if a 2DOF system is assumed, where

$$\lambda = -\frac{1}{2\alpha_0} \cdot (\alpha_1 \pm \sqrt{\alpha_1^2 - 4\alpha_0})$$

$$\alpha_0 = H_d^{xx}(\omega) \cdot H_d^{yy}(\omega) \cdot (\alpha_{xx}\alpha_{yy} - \alpha_{xy}\alpha_{yx})$$

$$\alpha_1 = \alpha_{xx} H_d^{xx}(\omega) + \alpha_{yy} H_d^{yy}(\omega)$$

here ω is the angular frequency at which H_d^{qq} has its minimal real value and

$$\alpha_{xx} = \frac{1}{2}\Big[\cos 2\phi - 2\frac{k_r}{k_t}\phi + \frac{k_r}{k_t}\sin 2\phi\Big]_{\phi_{st}}^{\phi_{ex}}$$

$$\alpha_{yy} = \frac{1}{2}\Big[-\cos 2\phi - 2\frac{k_r}{k_t}\phi - \frac{k_r}{k_t}\sin 2\phi \Big]_{\phi_{st}}^{\phi_{ex}}$$

$$\alpha_{xy} = \frac{1}{2}\Big[-\sin 2\phi - 2\phi + \frac{k_r}{k_t}\cos 2\phi \Big]_{\phi_{st}}^{\phi_{ex}}$$

$$\alpha_{xx} = \frac{1}{2}\Big[-\sin 2\phi + 2\phi + \frac{k_r}{k_t}\cos 2\phi \Big]_{\phi_{st}}^{\phi_{ex}}$$

$$\kappa = \frac{\Im\{\lambda\}}{\Re\{\lambda\}}$$

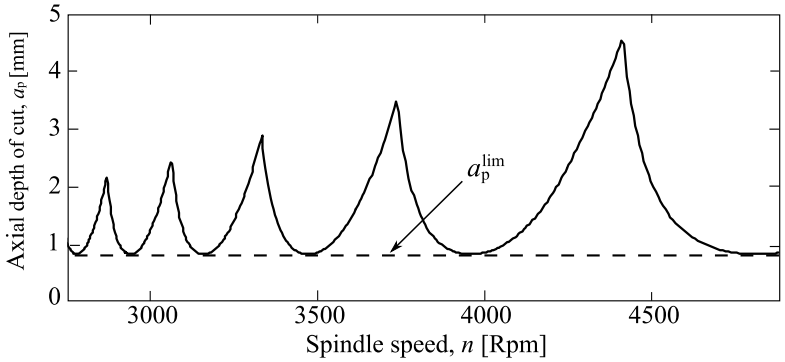

Figure 2.4: Shows the connection between a_p^{lim} and the stability lobes. Cutting operations with a_p below the solid black curve will be stable, while cutting operations with a_p above this curve will be unstable

2.3 Measurements of cutting forces

The two sensor types used to measure during cutting operations throughout this thesis are piezoelectric and strain gauges sensors. In the multi component dynamometer and the rotating multi component dynamometer the sensor type are piezoelectric and in the sensor equipped tool holders the sensor type is strain gauges. A more profound comparison of different techniques for cutting force measurements is available in [6].

2.3.1 Piezoelectric sensors

Piezoelectric sensors are made of material that when subjected to a force a charge displacement occurs, which can be measured. A commonly used piezoelectric material is quartz. Using piezoelectric sensors is the most common way of measuring multi component cutting forces [6].

In quartz, which is the material used in the multi component dynamometers, there are three piezoelectric effects: the longitudinal effect, transverse effect, and shear effect [12]. For the longitudinal effect the charge is proportional to the force acting on the piezoelectric object according to

$$C_q = d_{qq} F_q \tag{2.12}$$

where d is a piezoelectric constant [pC/N]. This is shown in figure 2.5a. For the transverse effect the charge can be formulated as

$$C_q = d_{qq'} F_q \cdot \frac{a}{b} \tag{2.13}$$

where d is a transverse piezoelectric constant, q' is the orthogonal direction to q, a is the charge generation axis, and b is the neutral axis. Shown in figure 2.5b. The shear effect can be formulated as

$$C_q = 2 d_{qq} F_q \tag{2.14}$$

as shown in figure 2.5c.

In the piezoelectric multi component dynamometer used in this thesis the quartz crystals are organised in thin plates, which are used to measure the force and the bending moment acting on the multi component dynamometer.

A piezoelectric material yields electric charge when a force is exerted on it. A readable voltage that is proportional to the force acting on the piezoelectric elements can be obtained by connecting a charge amplifier to the multi component dynamometer. The constant d_{qq} in equation 2.12 is used in the charge amplifier in order to get the correct amplification. The entire connection setup is shown in figure 2.6. For more in-depth information on piezoelectric sensors see [12], [13], and [14].

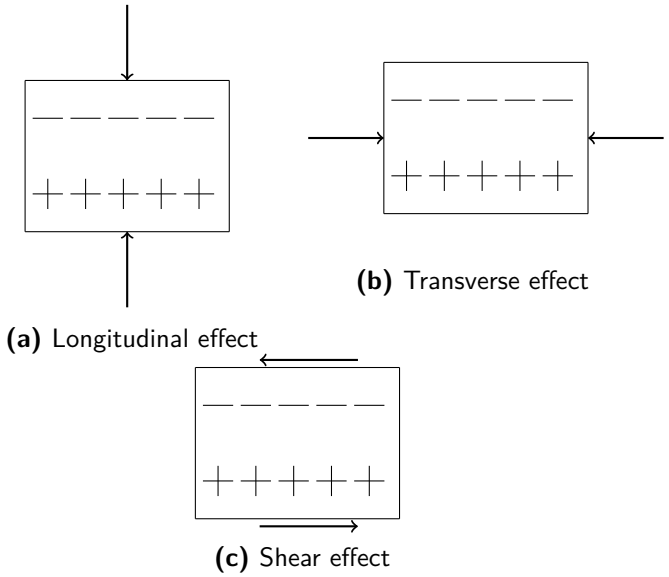

Figure 2.5: The three types of piezoelectric effect

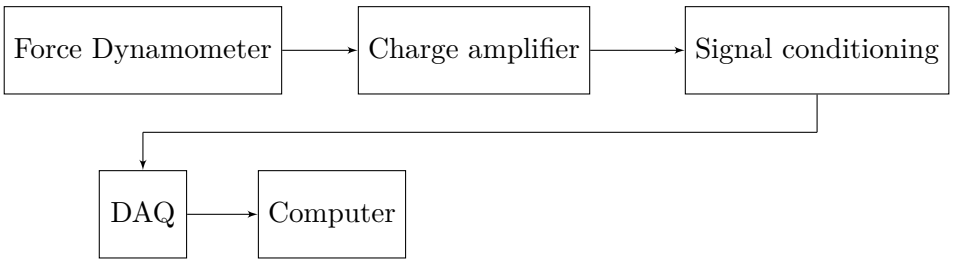

Figure 2.6: Data flow for the piezoelectric measurement equipment

2.3.2 Strain gauges

Strain gauges works by the principle that its electrical resistance changes when its area changes. Due to the design of the strain gauge, its electrical resistance is mainly sensitive to size change in one direction; change in the orthogonal direction does not affect its resistance. A common way of measuring this change is by connecting the strain gauge in a full bridge connection, as seen in figure 2.7. For this setup, the voltage U_1 is dependent on the current value of R_1, R_2, R_3, and R_4. For the sensor equipped tool holders used the strain gauges are not presenting measured forces in radial or tangential direction, instead the accompanying software presents the bending moment acting on them, M_t and M_r. There is however a strain gauge mounted in such way that it is sensitive to force acting in the axial direction, F_z. Despite not measuring the force, it can be calculated knowing the

bending moment in a direction, M_q. The force acting on the tool in that direction, F_q, can be calculated as

$$F_q = \frac{M_q}{L} \tag{2.15}$$

where L is the distance from the tool tip to the strain gauges. The value of L for the two tool holders in the conducted experiments is shown in table 2.1.

	Tool holder A	Tool holder B
L	71 mm	96 mm

Table 2.1: L for the two sensor equipped tool holders

	Tool holder A	Tool holder B
F_z	6.527 94	2.754 85
Torque	0.044 342 7	0.020 628 3
M_r	0.026 61	0.014 879 4
M_t	0.026 502 7	0.015 013 8

Table 2.2: Calibration values for the two sensor equipped tool holders

The mounting of the strain gauge is of particular importance to assure proper functionality. Each strain gauge has a specified linear measuring range. If placed in a position where the strain exceeds this range, inaccurate measurements will follow and in worst case the strain gauge detaches from the mounting surface. The specified measuring range for each tool holder is shown in table 2.3.

	Tool holder A	Tool holder B
Axial force	±88.7 kN	±34.7 kN
Torque	±602.4 N m	±280.2 N m
Bending moment	±360 N m	±203.9 N m
Max speed	18 000 RPM	18 000 RPM

Table 2.3: Specified measuring ranges for the sensor equipped tool holders

Due to the mounting of the strain gauges in the sensor equipped tool holders, both the number of revolutions per minute and temperature changes affects the reading. This since both increased RPM and temperature causes the tool holder to expand, and thereby changing the size of the strain gauges. This can be compensated for

by assuming that there is a constant offset and reset at what is the new zero-level. Another phenomena that may occur is drift during measurements, then every sample is adjusted according to a linear model of the drift. Investigations of how much the drift affects the measurements, or if the drift is purely linear has been left out due to thesis limitations.

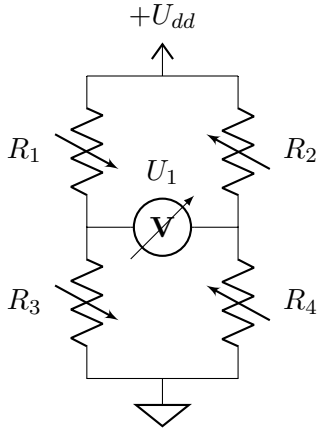

Figure 2.7: Schematic strain gauge sensor coupling in a full bridge where R_1 is the strain gauge, U_1 is measured

2.4 Design of inverse filter

The inverse filter obtained is based on the multi component dynamometers measured FRF, with a modification to ensure stability and invertability. This modification of the FRF is conversion to its minimum phase representation, which also entails that the approximated filter will be minimum phase. Without this conversion the inverse filter would not be stable. Since using filtering may cause phase distortions, a filtering method for removing this, named zero phase filtering, is used when applicable.

2.4.1 Stability properties

With stability of a filter it means that the filter is BIBO-stable, *i.e.* bounded input gives a bounded output. This is a highly desired property. Let $h(n)$ be the impulse response of a filter, the filter is then stable if the following constrain holds true [15, p. 88]

$$\sum_{n=-\infty}^{\infty} |h(n)| = ||h||_1 < \infty \tag{2.16}$$

This can be expressed in the z-domain, given that the filter transfer function in the z-domain is written as

$$H(z) = \frac{B(z)}{A(z)} \tag{2.17}$$

where $B(z)$ and $A(z)$ are the numerator and denominator polynomials, respectively. The filter is unstable if $A(z)$ has roots outside the unit circle.

2.4.2 Minimum phase

A filter, $H(z)$, is said to be a minimum phase filter if all roots of $A(z)$ and $B(z)$ are within the unit circle, which can be expressed as

$$\max\{|n_i|\} < 1 \quad \text{and} \quad \max\{|p_i|\} < 1$$

Given a non-minimum phase filter on the form as in equation 2.17, by reflecting all of its zeros outside the unit circle inside of the unit circle transforms the filter to its minimum phase representation can be achieved by

$$n_i = \frac{n_i}{|n_i|^2} \tag{2.18}$$

The magnitude response is unchanged by this operation, though it changes the phase response. If the FRF of the filter is known and the $H(z)$ is unknown, the transformation to its minimum phase representation can be made by using the FRFs real and complex cepstrum. A method which was presented by Soo-Chang Pei and Huei-Shan Lin in [16]. Given a causal real valued sequence, $h(n)$, which Fourier transform is $H(\omega)$ the method is as follows. Let $\hat{h}(n)$ be the complex cepstrum of $h(n)$, the Fourier transform of $\hat{h}(n)$ is obtained as

$$\hat{H}(\omega) = \log[H(\omega)] \tag{2.19}$$

The Fourier transform of $h(n)'s$ real cepstrum is

$$\hat{C}(\omega) = \Re e[\hat{H}(\omega)] \tag{2.20}$$

which gives that the real cepstrum is

$$\hat{c}(n) = \mathscr{F}^{-1}\{\hat{C}(\omega)\} \tag{2.21}$$

Since $h(n)$ is a casual sequence its minimum phase representation, $h_{\min}(n)$, is then obtained as

$$\hat{h}_{\min}(n) = \begin{cases} 0 & n < 0 \\ \hat{c}(n) & n = 0 \\ 2\hat{c}(n) & n > 0 \end{cases}$$

and reversing equation 2.19, the minimum phase FRF is then acquired as

$$H_{\min}(\omega) = e^{\mathscr{F}\{\hat{h}_{\min}(n)\}} \tag{2.22}$$

$H_{min}(\omega)$ is the minimum phase representation of $H(\omega)$. This is the method that was used through out this thesis. If a filter, $H(z)$, is in its minimum phase representation the denominator and numerator can be switched, without causing instability. Given a minimum phase filter as

$$H(z) = \frac{B(z)}{A(z)}$$

it has the BIBO-stable inverse

$$H^{-1}(z) = \frac{A(z)}{B(z)}$$

2.4.3 Zero phase filtering

By using forward-backward filtering it is possible to achieve zero phase-distortions with IIR-filters, this is achieved when the filter is first applied forwards and then backwards [17]. The output from a filter with input $x(n)$ and impulse response $h(n)$ can in frequency domain be written as

$$Y(\omega) = X(\omega) \cdot H(\omega)$$

Applying the same filter once again from the negative direction can hence be expressed as

$$Y(\omega) = X(\omega) \cdot H(\omega) \cdot H(-\omega) \tag{2.23}$$

which for a filter with real value coefficients is

$$Y(\omega) = X(\omega) \cdot H(\omega) \cdot H^*(\omega) = X(\omega) \cdot |H(\omega)|^2 \tag{2.24}$$

where $H^*(\omega)$ is the complex conjugate of $H(\omega)$. As seen in equation 2.24 the output has zero phase distortions, since $|H(\omega)|^2$ is real valued. It however changes the cut off-frequency, which affects the filter design. Throughout this thesis the type of filter used for low pass filtering was Butterworth-filters, for this reason only the effect on Butterworth-filter from zero phase filtering is covered. For a Butterworth filter of n:th-order the gain is [18]

$$G_{\text{butter}}(\omega) = |H_{\text{butter}}(i\omega)| = \frac{1}{\sqrt{1 + (\frac{\omega}{\omega_c})^{2n}}} \tag{2.25}$$

using the result from equation 2.24 yields

$$G_{\text{zero phase}}(\omega) = \frac{1}{1 + (\frac{\omega}{\omega_c})^{2n}} \tag{2.26}$$

from equation 2.25 and 2.26 it can be shown that the new cut off-frequency is

$$\omega_{\text{new c}} = (\sqrt{2} - 1)^{\frac{1}{2n}} \cdot \omega_c \tag{2.27}$$

2.4.4 Filter fitting

Assuming a minimum phase FRF as described in subsection 2.4.2 and given a measured FRF, $H(\omega)$, an approximation of this $H(\omega)$ is found by minimising the following error function

$$E = \sum_{k=1}^{S_n} \left| H(\omega_k) - \frac{B(\omega_k)}{A(\omega_k)} \right| \tag{2.28}$$

This is performed by first by minimising equation 2.29

$$E = \sum_{k=1}^{S_n} |A(\omega(k))H(\omega(k)) - B(\omega(k))|^2 \tag{2.29}$$

where A and B are polynomials, and S_n is the number of samples in the measured FRF, with respect to A and B. The method used to do this is presented in [19] and is as follow. Define the estimated transfer function $G(i\omega)$ as

$$G(i\omega) = \frac{A_0 + A_1(i\omega) + A_2(i\omega)^2...}{B_0 + B_1(i\omega) + B_2(i\omega)^2...} \tag{2.30}$$

where $B_0 \equiv 1$ and the error as the difference between the measured and estimated

$$\epsilon(\omega) = H(\omega) - G(\omega) \tag{2.31}$$

$G(\omega)$ can be re-written as $\frac{B(\omega)}{A(\omega)}$ then

$$A(\omega)\epsilon(\omega) = A(\omega)H(\omega) - B(\omega) \tag{2.32}$$

Re-writing the right hand side of equation 2.32 as a sum of its real and imaginary parts yields

$$A(\omega)\epsilon(\omega) = a(\omega) + ib(\omega) \tag{2.33}$$

thus the error E can be defined as

$$E = \sum_{k=1}^{S_n} a^2(\omega_k) + b^2(\omega_k) \tag{2.34}$$

where a and b is a function of both ω and the unknown coefficients A_i and B_i, and n is the number of sample points. If $G(i\omega)$ is expressed as

$$G(i\omega) = \frac{\alpha + i\omega\beta}{\sigma + i\omega\tau} \tag{2.35}$$

where

$$\alpha = A_0 - A_2\omega^2 + A_4\omega^4...$$

$$\beta = A_1 - A_3\omega^2 + A_5\omega^4...$$

$$\sigma = B_0 - B_2\omega^2 + B_4\omega^4...$$

$$\tau = B_1 - B_3\omega^2 + B_5\omega^4...$$

then equation 2.34 may be written as

$$E = \sum_{k=1}^{S_n} (\sigma_k \cdot \Re\{H(\omega_k)\} - \alpha_k - \Im\{H(\omega_k)\} \cdot \omega_k \cdot \tau_k)^2 + (\Im\{H(\omega_k)\} \cdot \sigma_k + \Re\{H(\omega_k)\} \cdot \omega_k \cdot \tau_k - \omega_k \cdot \beta_k)^2 \tag{2.36}$$

Differentiating equation 2.36 with respect to A_i and B_i yields the following set of equations

$$\frac{\partial E}{\partial A_0} = \sum_{k=1}^{S_n} -2 \cdot a_k, \quad \frac{\partial E}{\partial A_1} = \sum_{k=1}^{S_n} -2 \cdot \omega_k \cdot b_k, \quad \frac{\partial E}{\partial A_2} = \sum_{k=1}^{S_n} 2 \cdot \omega_k^2 \cdot a_k \quad ...$$

$$\frac{\partial E}{\partial B_1} = \sum_{k=1}^{S_n} [-2 \cdot \omega_k \cdot a_k \cdot \Im\{H(\omega_k)\} + 2 \cdot \omega_k \cdot b_k \cdot \Re\{H(\omega_k)\}],$$

$$\frac{\partial E}{\partial B_2} = \sum_{k=1}^{S_n} [-2 \cdot \omega_k^2 \cdot a_k \cdot \Re\{H(\omega_k)\} - 2 \cdot \omega_k^2 \cdot b_k \cdot \Im\{H(\omega_k)\}],$$

$$\frac{\partial E}{\partial B_3} = \sum_{k=1}^{S_n} [2 \cdot \omega_k^3 \cdot a_k \cdot \Im\{H(\omega_k)\} - 2 \cdot \omega_k^3 \cdot b_k \cdot \Re\{H(\omega_k)\}]$$

$$\vdots$$

Setting all of the above equations to 0 and using the linear transformations given in [19] yields a set of linear equations that may be written in matrix form as

$$M \cdot N = C \tag{2.37}$$

where

$$M = \begin{pmatrix} \lambda_0 & 0 & -\lambda_2 & 0 & \cdots & T_1 & S_2 & -T_3 & -S_4 & \cdots \\ 0 & \lambda_2 & 0 & -\lambda_4 & \cdots & -S_2 & T_3 & S_4 & -T_5 & \cdots \\ \lambda_2 & 0 & -\lambda_4 & 0 & \cdots & T_3 & S_4 & -T_5 & -S_6 & \cdots \\ \vdots & \vdots & \vdots & \vdots & \vdots & \vdots & \vdots & \vdots & \vdots & \vdots \\ T_1 & -S_2 & -T_3 & S_4 & \cdots & U_2 & 0 & -U_4 & 0 & \cdots \\ S_2 & T_3 & -S_4 & -T_5 & \cdots & 0 & U_4 & 0 & -U_6 & \cdots \\ T_3 & -S_4 & -T_5 & S_6 & \cdots & U_4 & 0 & -U_6 & 0 & \cdots \\ \vdots & \vdots & \vdots & \vdots & \vdots & \vdots & \vdots & \vdots & \vdots & \vdots \end{pmatrix} \tag{2.38}$$

and where

$$N = \begin{pmatrix} A_0 & A_1 & A_2 & \cdots & B_1 & B_2 & B_3 & \cdots \end{pmatrix}^T \tag{2.39}$$

and

$$C = \begin{pmatrix} S_0 & T_1 & S_2 & \cdots & 0 & U_2 & 0 & \cdots \end{pmatrix}^T \tag{2.40}$$

Thus

$$N = M^{-1} \cdot C \tag{2.41}$$

The elements of N is the coefficients that minimises equation 2.32.

The solution obtained from equation 2.41 is used as the initial guess in the damped Gauss-Newton [20] iterative search for the minimal value of the error function

$$E = \sum_{k=1}^{S_n} \left| H(\omega_k) - \frac{B(\omega_k)}{A(\omega_k)} \right| \tag{2.42}$$

which is minimised by the iterative scheme

$$\bar{x}_{i+1} = \bar{x}_i - \lambda_i \big(J(\bar{x}_i)^T \cdot J(\bar{x}_i) \big)^{-1} \cdot J(\bar{x}_i)^T \cdot R(\bar{x}_i) \tag{2.43}$$

The reason that the coefficients which minimises 2.29 is not used as filter coefficients is since they do not guarantee stability. In this thesis this was performed with MATLAB using the built-in function `invfreqz`.

Chapter 3
Method

This thesis is performed in several steps in order to make an as good evaluation of the sensor equipped tool holders as possible.

At first the dynamic behaviour of both the un-modified and sensor equipped tool holders A and B, with dummy tools mounted, is measured. This yields a FRF for each setup of the tool holders, that has been used to predict the critical depth of cut, $a_{\mathrm{p}}^{\mathrm{lim}}$, with respect to cutting process parameters and selected work piece material [9]. A comparison between the un-modified and sensor equipped tool holders A and B dynamic characteristics is made, this to evaluate how much the dynamic behaviour of the tool holder is affected after sensor integration.

During the previous mentioned measuring of dynamic characteristics the force impulse response from the multi component force dynamometer, and sensor equipped tool holder A and B is recorded. This is used to approximate the FRF with an IIR-model, the model is then used to obtain an inverse model that can be used to reduce the dynamic influence on cutting force measurements.

The performance evaluation of the mounted sensors was conducted by the same milling and drilling operation for both sensor equipped tool holders A and B. The output from the sensor equipped tool holders is compared to a theoretical simulation and measurement data acquired from a multi component dynamometer. This test was repeated for several variations of cutting parameters. For the drilling experiments, the measurements from the sensor equipped tool holders is compared with measurement data from both a stationary multi component dynamometer and a rotating multi component dynamometer.

3.1 Measurement of the tool holders dynamic behaviour

There were in total eight dynamic measurements performed on the tool holders, two for each tool holder; un-modified tool holder A and B, and sensor equipped tool holder A and B. The first measurement per tool holder was performed with a blank 20 mm diameter tool, while the second measurement was with a blank 12 mm diameter tool. A principal sketch of how the sensor system was mounted on the tool holders is seen in figure 3.1.

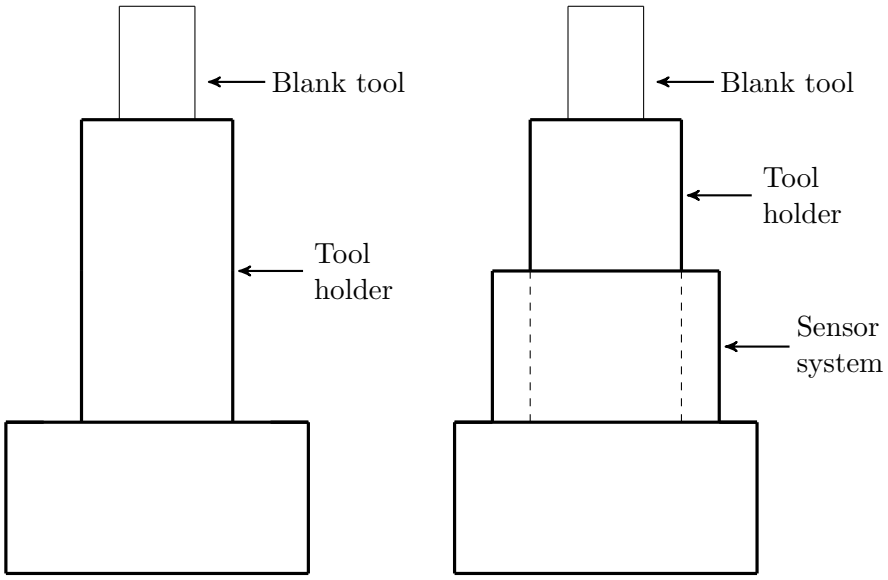

(a) Tool holder without sensor system **(b)** Tool holder with sensor system

Figure 3.1: Principal sketch over how the sensor system was mounted on the tool holders

The purpose of the following measurements was to measure the dynamic behaviour of the tool holders and obtain H_d for calculation of $a_{\mathrm{p}}^{\mathrm{lim}}$. The tool holders were mounted in a test rig as seen in figure 3.2, while figure 3.3 shows how the measurement equipment was connected.

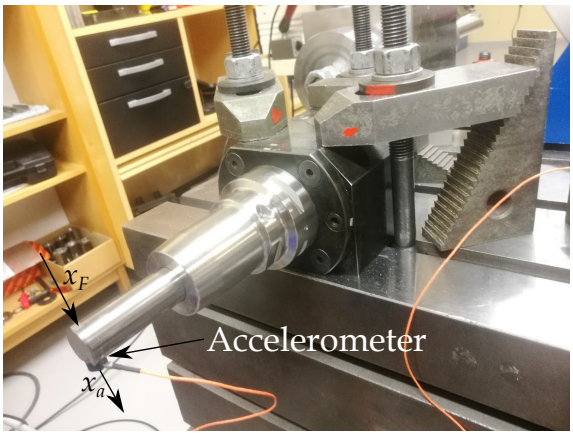

Figure 3.2: Measurement setup, with un-modified tool holder A and dummy tool, to measure tool holder dynamics

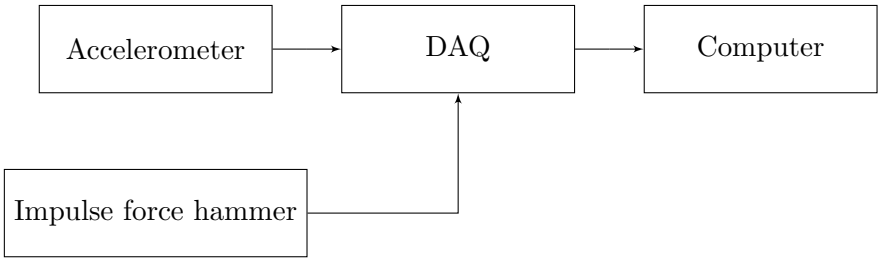

Figure 3.3: The data flow during the measurements

An impulse force hammer was used to strike the tip of the dummy tool, thus yielding both an input force signal, $x_F(t)$, and the output acceleration signal, $x_a(t)$, that was registered by an accelerometer mounted on the opposite side of the blank tool tip. These signals were then used to calculate $a_{\mathrm{p}}^{\mathrm{lim}}$ as described in section 2.2.

3.2 Measurement of multi component dynamometer dynamic behaviour

The multi-component dynamometer was mounted as seen in figure 3.4 and connected as seen in figure 3.5. As opposed to the measurements on the tool holders where an accelerometer was used in order to measure the output, the multi component dynamometers force signal was used. This means that the transfer function was force to force, and not force to acceleration as for the tool holder measurements.

The impulse force hammer was used to strike the workpiece mounted on the multi component force dynamometer in both x and y direction and the force output in the respective direction was recorded. This yielded an input force signal $x_F^{\mathrm{i}}(t)$ and an output signal $x_F^{\mathrm{o}}(t)$, using the same procedure as the tool holders a transfer function measurements

$$H(\omega) = \frac{X_F^{\mathrm{o}}(\omega)}{X_F^{\mathrm{i}}(\omega)} \tag{3.1}$$

Here it should be noted that no integration was performed, as it was for the tool holders, since the desired transfer function was directly obtained.

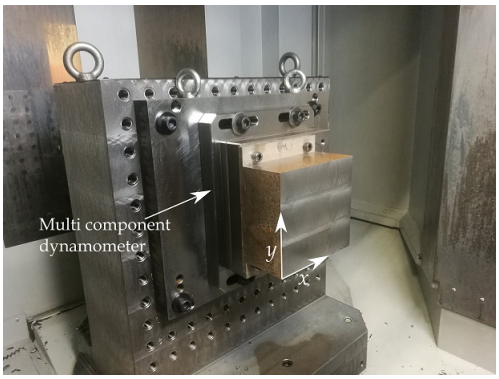

Figure 3.4: The multi-component dynamometer with workpiece mounted in CNC-machine

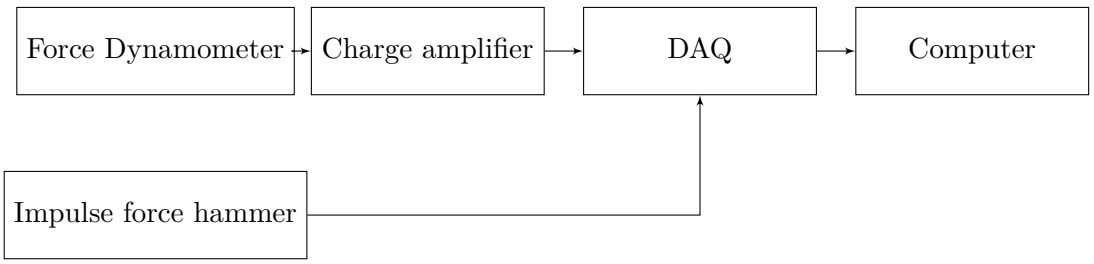

Figure 3.5: Schematic connection description of multi component force dynamometer during measurements of dynamic behaviour

3.3 Reduction of dynamic influence

A method for obtaing an inverse filter for milling applications was presented by M. Magnevall *et al.* in [21], this method is the method that is used in this thesis. Similiar methods can be found in the literature and examples of such using Kalman-filters have been researched in [5] [22]. Using the theory described in subsection 2.4.2 and subsection 2.4.4, together with the method presented in [21] to

obtain a minimum phase-representation of the FRFs in 4.2a and 4.2b. The FRFs were approximated using a filter as

$$H_{qq}^{\text{est}}(z) = \frac{A_0 + A_1 z^{-1} + .. + A_{400} z^{-400}}{1 + B_1 z^{-1} + ... + B_{50} z^{-50}} \tag{3.2}$$

Switching the numerator and denominator in H_{qq}^{est} yields the inverse filter in the respective direction. As the filter is approximated using the sample rate used of dynamic measurements, a re-sampling of the cutting force signal is necessary if the sample rate is different. The data flow through the filters is shown in figure 3.6.

Figure 3.6: The flow of the data through the filters

All the filtering with low pass-filters were made using the zero phase filtering method, described in subsection 2.4.3 and the cut off frequency was adjusted as in equation 2.27.

3.4 Performance measurements of sensor equipped tool holders

Using the software provided with the sensor equipped tool holder, the toolholder was connected as in figure 3.7. The wireless connection was with radio at the 2.4 GHz band with 16 channels. For the milling tests the sensor equipped tool holders were compared against the stationary multi component dynamometer; which was connected as in figure 3.8. The cutting parameters used for all milling tests performed were

- Cutting tool: R331.35-050A20EM100
- Instert: N331.1A-08 45 08M-PM4230
- Workpiece: 34CrNiMo6
- z = 1
- $\gamma = -20$
- $v_c = 220\,\mathrm{m/min}$
- $a_\mathrm{p} = 3\,\mathrm{mm}$
- $a_e = 5\,\mathrm{mm}$, $10\,\mathrm{mm}$, $25\,\mathrm{mm}$ and $50\,\mathrm{mm}$
- $f_z = 0.05\,\mathrm{mm}$, $0.1\,\mathrm{mm}$ and $0.15\,\mathrm{mm}$

The selection of only one cutting tooth and fixed values of v_c, a_p, a_e, and f_z provides periodic and well separated cutting engagements.

In the drilling tests both a stationary and rotating multi component dynamometer were used as references, the stationary multi component was used for measuring F_z and the rotating for measuring torque. The rotating multi component dynamometer was also connected as in figure 3.8. The following were the cutting parameters for the drill tests

- Drill: R840-1200-30-A0A 1220
- Workpiece: 34CrNiMo6
- $v_c = 80\,\mathrm{m/min}$
- $f_n = 0.12\,\mathrm{mm}$ and $0.2\,\mathrm{mm}$

Figure 3.7: Connection of sensor equipped tool holder

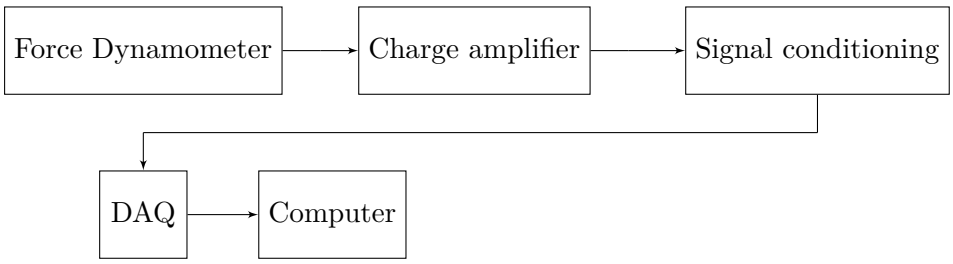

Figure 3.8: Connection of external multi component dynamometers

Chapter 4
Results

The results presented in this chapter are: the critical depth of cut for each tool holder, FRFs for the multi component dynamometer, implementation and result of filter for reduction of dynamic influence, and a comparison between the sensor equipped tool holders with a multi component dynamometer.

4.1 Dynamic behaviour of tool holders

In the calculations of $a_{\mathrm{p}}^{\mathrm{lim}}$ it was assumed that $H_{xx} = H_{yy}$, which is not entirely true despite the tool holders being cylindrical. Yet, this assumption makes for a valid evaluation of the tool holder performance. The calculated critical depth of cut for all tool holders, both sensor equipped and un-modified, for $\phi_{st} = \pi/2\,\mathrm{rad}$ and $\phi_{ex} = \pi\,\mathrm{rad}$, is shown in table 4.1 and 4.2. The cutting force coefficients used were $k_r = 405\,\mathrm{N/mm^2}$ and $k_t = 1370\,\mathrm{N/mm^2}$ which were derived from turning tests in the workpiece material 34CrNiMo56. $\Re\{H_d\}$ for all tool holders is shown in figure 4.1. The coherence- and FRF-plots are avalible in appendix A.

	Tool holder A	Tool holder B	Sensored tool holder A	Sensored tool holder B
$a_{\mathrm{p}}^{\mathrm{lim}}$	5.15 mm	3.69 mm	5.32 mm	4.03 mm

Table 4.1: Shows $a_{\mathrm{p}}^{\mathrm{lim}}$ for all tool holder with 12 mm dummy tool

	Tool holder A	Tool holder B	Sensored tool holder A	Sensored tool holder B
$a_{\mathrm{p}}^{\mathrm{lim}}$	2.93 mm	2.93 mm	4.77 mm	7.44 mm

Table 4.2: Shows $a_{\mathrm{p}}^{\mathrm{lim}}$ for all tool holder with 20 mm dummy tool

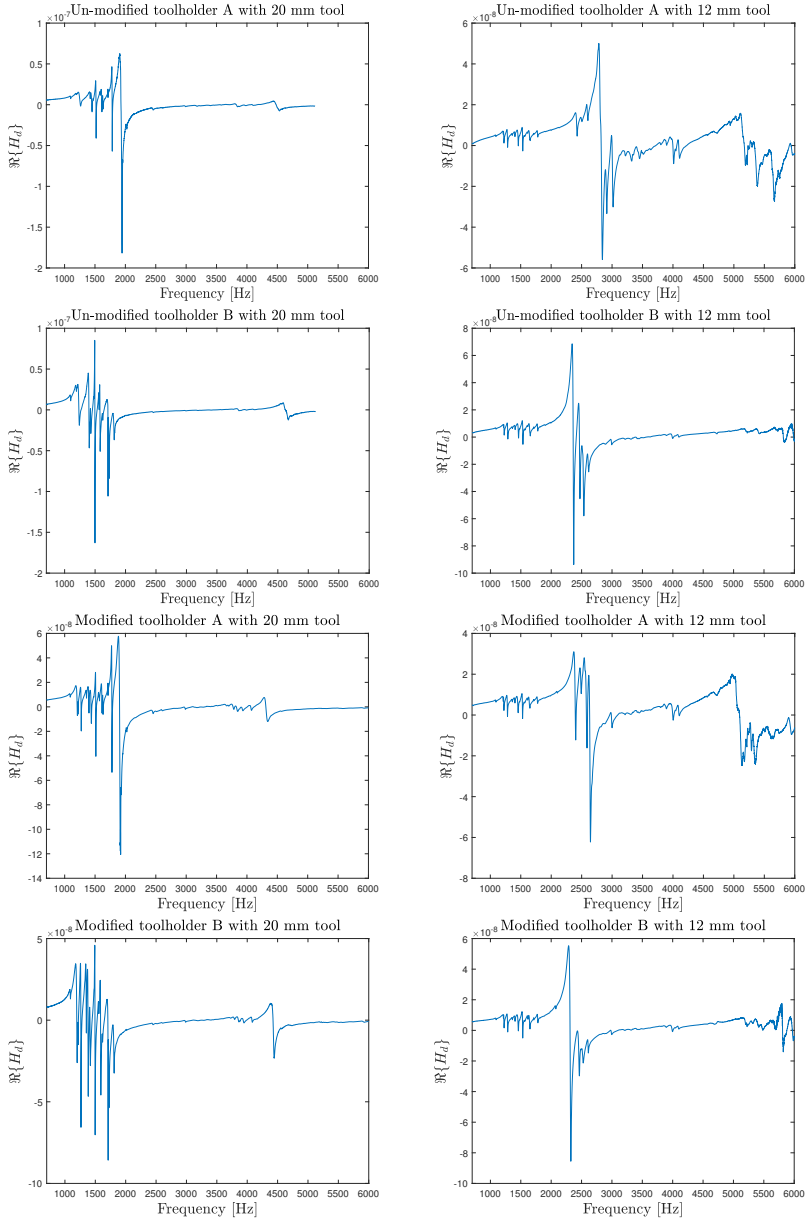

Figure 4.1: Shows $\Re\{H_d\}$ for all tool holders

4.2 Multi component dynamometer

Figure 4.2a - 4.3b shows the result from the measurements where the ideal result should be that $H(\omega) = 1$ for all frequencies, this is however not the case. The cross-transfer functions, H_{xy} and H_{yx}, are not of significant amplitude and therefor not shown. Figures 4.4a and 4.4b shows the phase after the FRF have been converted to its minimum phase representation using the method described in subsection 2.4.2.

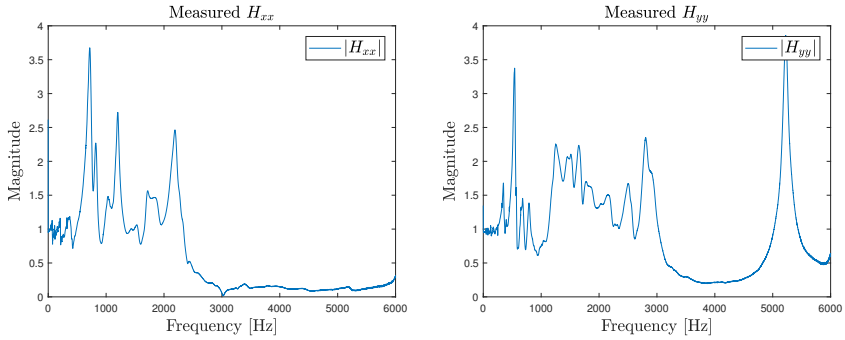

(a) $|H_{xx}|$ **(b)** $|H_{yy}|$

Figure 4.2: Amplitude of measured transfer functions for multi component dynamometer

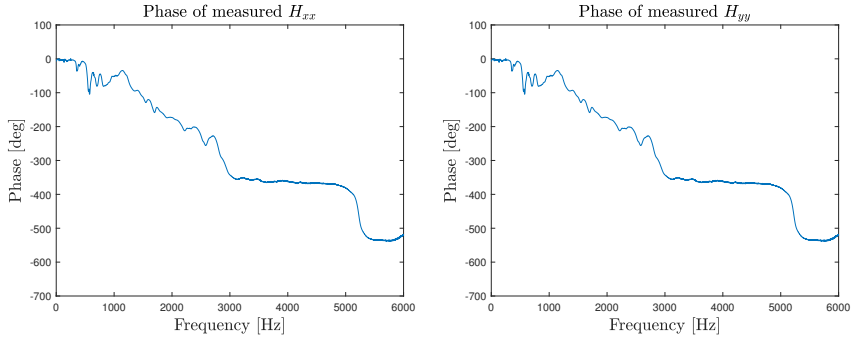

(a) Phase response of measured H_{xx} **(b)** Phase response of measured H_{yy}

Figure 4.3: Phase responses of measured transfer functions for multi component dynamometer

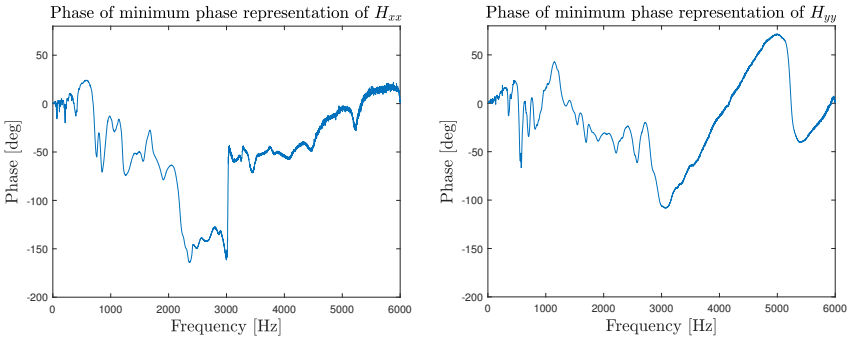

(a) Phase response H_{xx}^{min} **(b)** Phase response H_{yy}^{min}

Figure 4.4: Phase responses of the minimum phase representations

4.3 Reduction of dynamic influence

As seen in figures 4.2a and 4.2b, the multi component force dynamometer significantly amplifies and attenuates certain frequencies, which causes a distortion in the measurements. This is a known phenomena and the current practice is to use a Butterworth low pass-filter to cut off frequencies above 250 Hz. This method leads to loss of information about the cutting forces. However, not applying a low pass-filter would mean that cutting force signal is distorted due to the workpiece and multi component dynamometers dynamic behaviour acting as a mechanical filter.

The approximations of the measured multi component dynamometers FRFs is shown in figure 4.5, in respective direction. The approximation closely matches the measured FRF. Switching numerator and denominator in H_{xx}^{est} and H_{yy}^{est} and filtering the recorded impulse response with the inverse filters yields the FRFs in figure 4.6. The phase response of the obtained inverse filter is seen in figure 4.7. As the phase is linear up to 2000 Hz the low pass-filter shown in 3.6 has the cut off-frequency set to $f_c = 2000$ Hz, this to avoid further signal distortion.

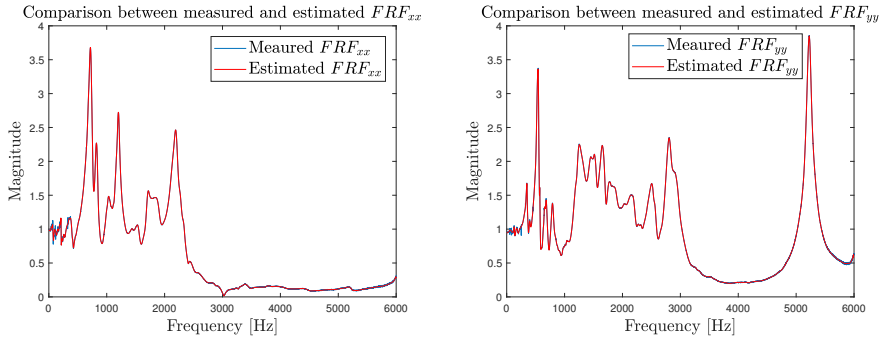

Figure 4.5: Left: approximation of FRF_{xx},H_{xx}^{est}
Right: approximation of FRF_{yy}, H_{yy}^{est}

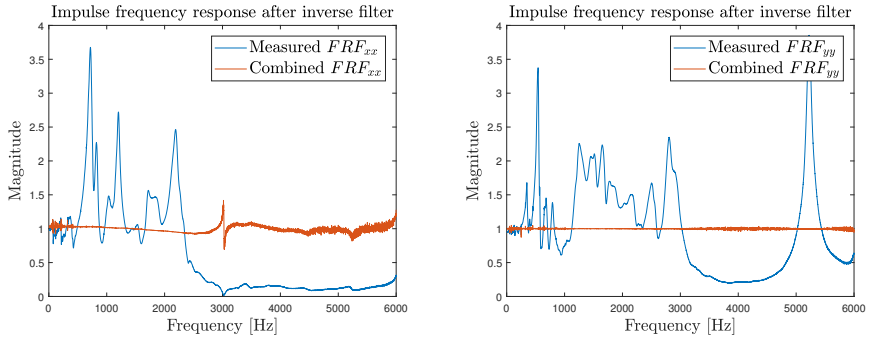

Figure 4.6: The FRF of the inverse filtered impulse response for each direction

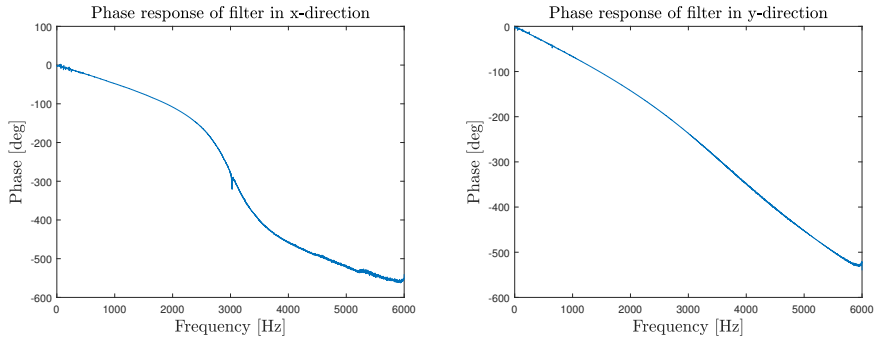

Figure 4.7: Phase response of inverse filters in respective direction

In figures 4.8-4.13 a comparison between the raw data, inverse and low pass-filtered data, simulation of milling operation and low pass-filtered data is displayed. For small radial engagement a_e, as in figure 4.9, the inverse filter reduces the oscillations without affecting the shape of the cutting force. As a comparison, the low pass-filter also reduces the amount of oscillations, however it also distorts the signal as seen in figure 4.9. For larger a_e, as figure 4.13, the difference between use of the inverse filter and the low pass-filter is not as significant as for smaller a_e. In figure 4.9 it is seen how the use of an inverse filter or low pass- filter reduces the dynamic influence from the multi component dynamometer. The oscillations in cutting force between the cutting engagements that can be seen in the measured raw data, does not exist; it is the multi component dynamometers dynamic behaviour that causes them. Under more detailed investigations it was noticed that the inverse filter in x-direction had a greater need of low pass-filtering, than the inverse filter in y-direction.

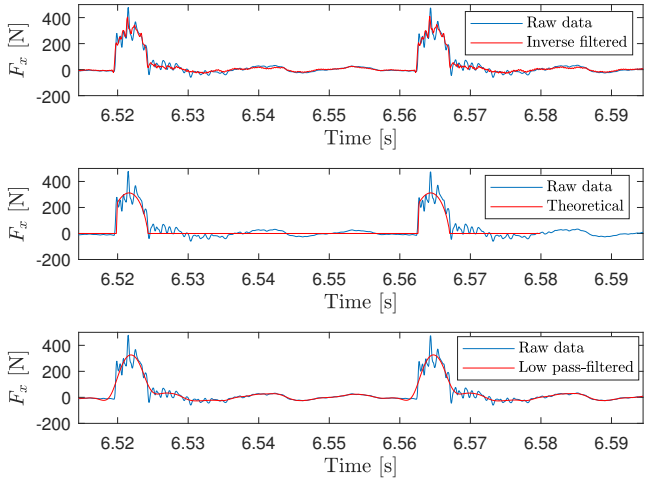

Figure 4.8: The comparison on F_x between the use of inverse filtered data, low pass filtered, measured raw data, and simulated milling force. $a_e = 5\,\text{mm}$, $f_z = 0.15\,\text{mm}$, $a_\text{p} = 3\,\text{mm}$, and $v_c = 220\,\text{m/min}$

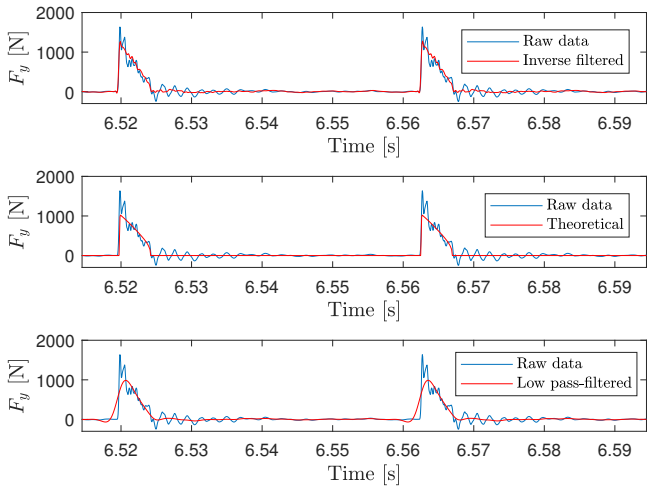

Figure 4.9: The comparison on F_y between the use of inverse filtered data, low pass filtered, measured raw data, and simulated milling force. $a_e = 5\,\mathrm{mm}$, $f_z = 0.15\,\mathrm{mm}$, $a_\mathrm{p} = 3\,\mathrm{mm}$, and $v_c = 220\,\mathrm{m/min}$

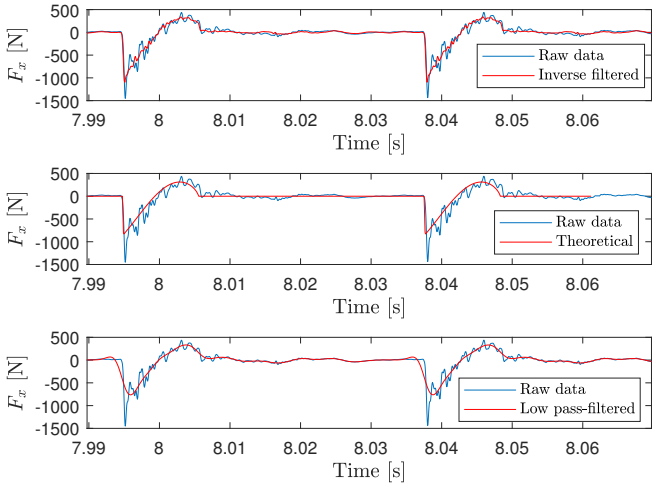

Figure 4.10: The comparison on F_x between the use of inverse filtered data, low pass filtered, measured raw data, and simulated milling force. $a_e = 25\,\mathrm{mm}$, $f_z = 0.15\,\mathrm{mm}$, $a_\mathrm{p} = 3\,\mathrm{mm}$, and $v_c = 220\,\mathrm{m/min}$

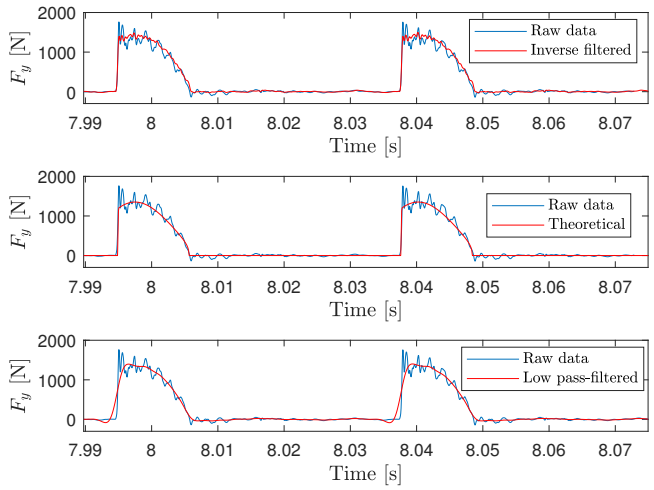

Figure 4.11: The comparison on F_y between the use of inverse filtered data, low pass filtered, measured raw data, and simulated milling force. $a_e = 25\,\mathrm{mm}$, $f_z = 0.15\,\mathrm{mm}$, $a_\mathrm{p} = 3\,\mathrm{mm}$, and $v_c = 220\,\mathrm{m/min}$

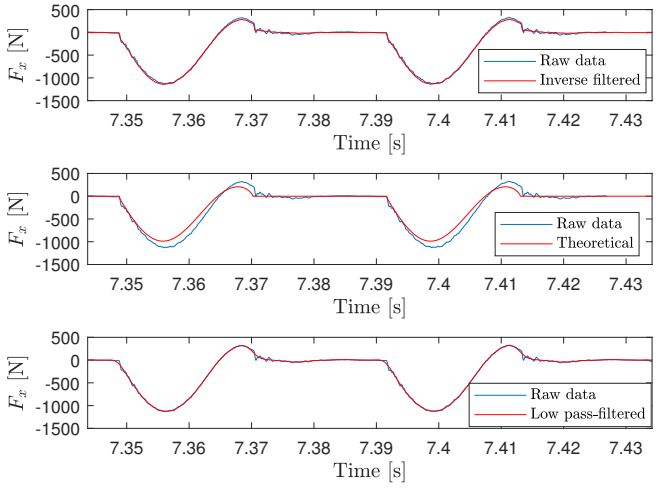

Figure 4.12: The comparison on F_x between the use of inverse filtered data, low pass filtered, measured raw data, and simulated milling force. $a_e = 50\,\mathrm{mm}$, $f_z = 0.1\,\mathrm{mm}$, $a_\mathrm{p} = 3\,\mathrm{mm}$, and $v_c = 220\,\mathrm{m/min}$

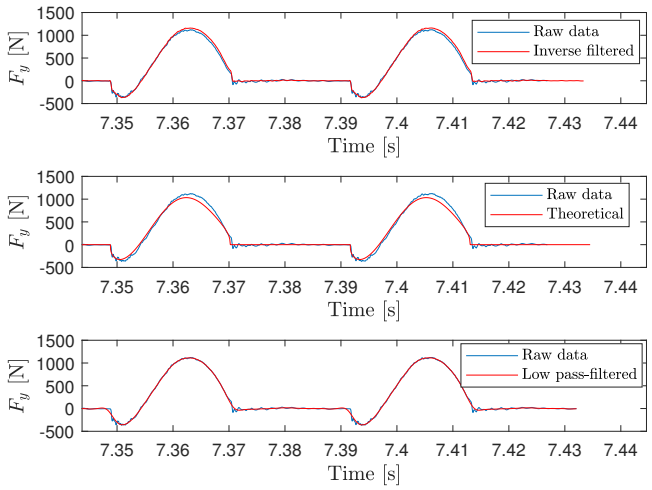

Figure 4.13: The comparison on F_y between the use of inverse filtered data, low pass filtered, measured raw data, and simulated milling force. $a_e = 50\,\mathrm{mm}$, $f_z = 0.1\,\mathrm{mm}$, $a_\mathrm{p} = 3\,\mathrm{mm}$, and $v_c = 220\,\mathrm{m/min}$

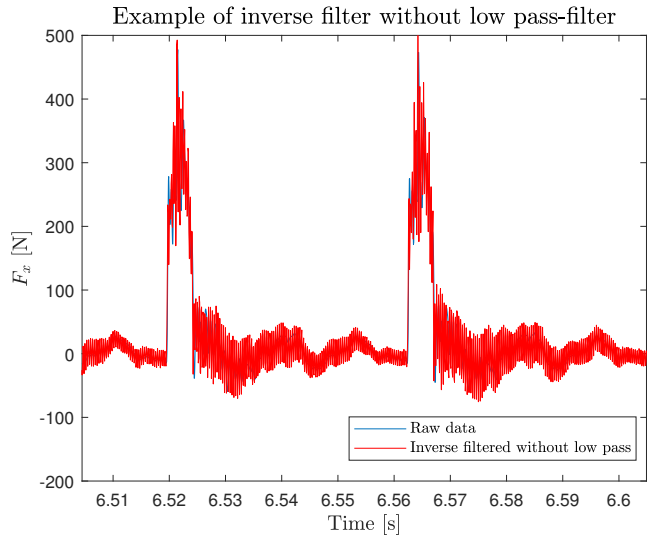

Figure 4.14: Same milling operation as in figure 4.8 without low pass-filter

4.4 Performance of sensor equipped tool holders

4.4.1 Milling

Figures 4.15-4.22 shows extracts of cutting force measurements with data obtained from sensor equipped tool holder A, compared with extracts from the inverse filtered data obtained with the multi component dynamometer. In figures 4.23 and 4.24 the total force, F_{tot}, obtained from sensor equipped tool holder A is shown for entire cutting operations. In figures 4.25-4.32 extracts of cutting force measurements obtained with sensor equipped tool holder B is shown. The total cutting force for two cutting operations obtained from sensor equipped tool holder B is shown in figures 4.34 and 4.36; the cutting parameters were the same as for figures 4.23 and 4.24, respectively. To compare the sensor equipped tool holders consistency the total force acquired with the multi component dynamometer for identical cutting operations as for the sensor equipped tool holders is shown in figures 4.33 and 4.35.

The sensor equipped tool holders also have the same kind of dynamic distortion of measurements as the multi component dynamometer, which can be seen in figure 4.25 and 4.27. Obtaining a filter similar to the one obtained for the multi component dynamometer is desirable. However, due to the low sampling rate, 2500 Hz, of the sensor equipped tool holders, a creation of such a filter was not possible as the sampling rate was too low to correctly capture the impulse forces.

Sensor equipped tool holder A

Some issues were observed with sensor equipped tool holder A where the sampling rate did not correspond to the time stamps. Therefor each sample was recalculated before the plots were made. The sample rate were not consistent, which is why the time between the cutting engagements, as in figure 4.18, varies. This problem is described in section 5.3.

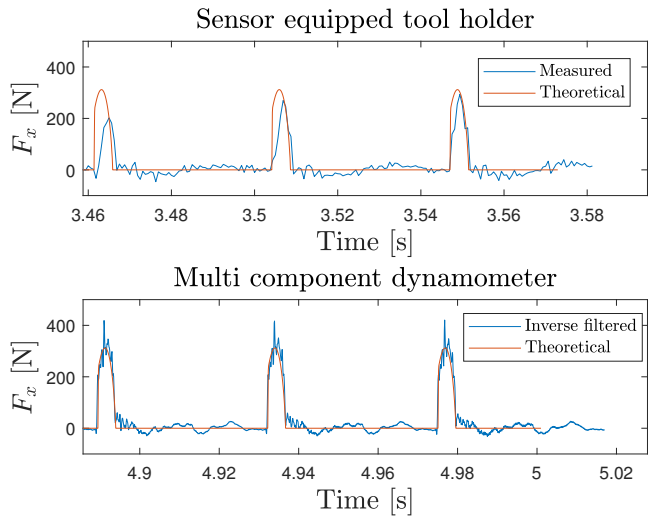

Figure 4.15: Comparison of F_x for top: sensor equipped tool holder A and bottom: multi component dynamometer with simulation for $a_e = 5\,\mathrm{mm}$, $f_z = 0.15\,\mathrm{mm}$, $a_\mathrm{p} = 3\,\mathrm{mm}$ and $v_c = 220\,\mathrm{m/min}$

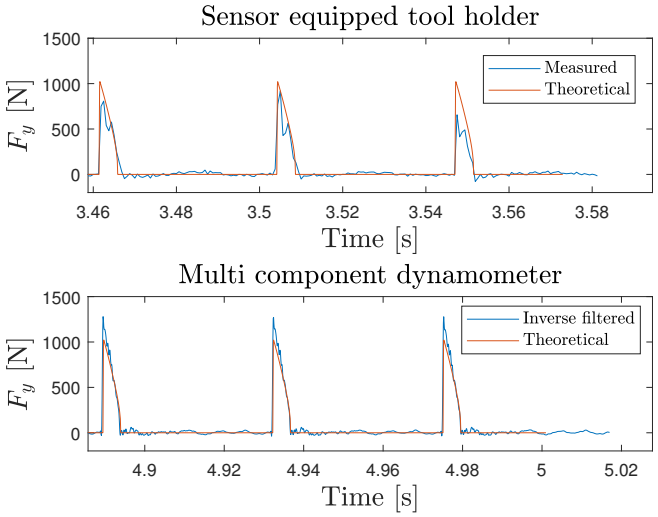

Figure 4.16: Comparison of F_y for sensor equipped tool holder A and bottom: multi component dynamometer with simulation for $a_e = 5\,\mathrm{mm}$, $f_z = 0.15\,\mathrm{mm}$, $a_\mathrm{p} = 3\,\mathrm{mm}$ and $v_c = 220\,\mathrm{m/min}$

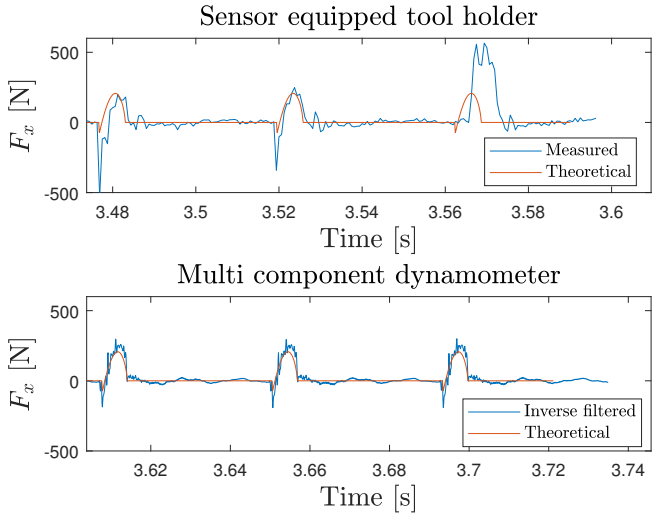

Figure 4.17: Comparison of F_x for top: sensor equipped tool holder A and bottom: multi component dynamometer with simulation for $a_e = 10\,\mathrm{mm}$, $f_z = 0.1\,\mathrm{mm}$, $a_\mathrm{p} = 3\,\mathrm{mm}$ and $v_c = 220\,\mathrm{m/min}$

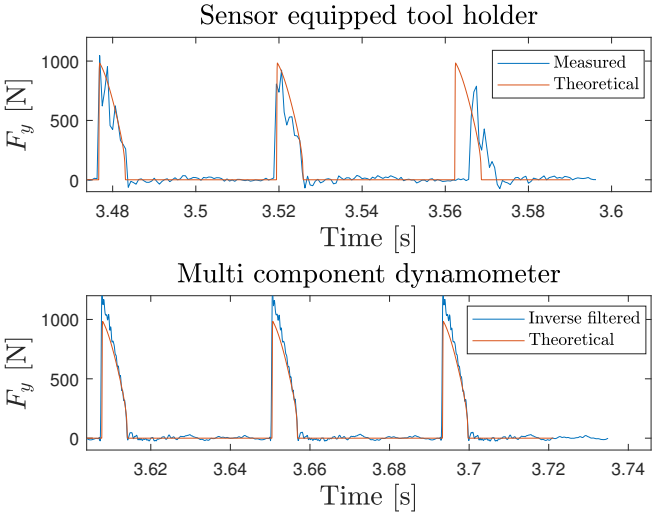

Figure 4.18: Comparison of F_y for top: sensor equipped tool holder A and bottom: multi component dynamometer with simulation for $a_e = 10\,\mathrm{mm}$, $f_z = 0.1\,\mathrm{mm}$, $a_\mathrm{p} = 3\,\mathrm{mm}$ and $v_c = 220\,\mathrm{m/min}$

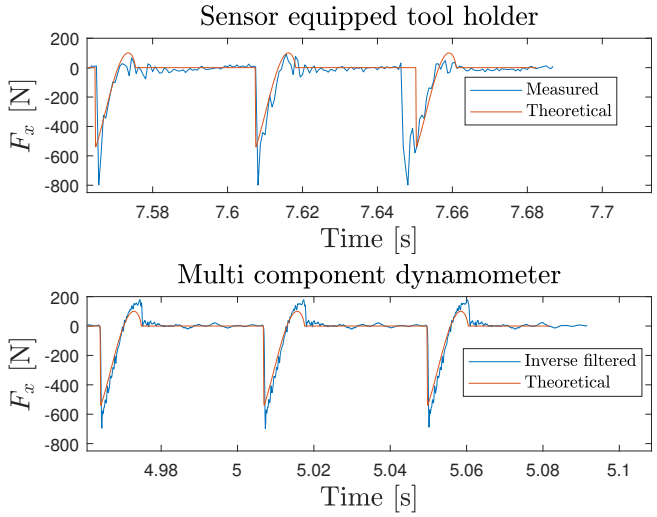

Figure 4.19: Comparison of F_x for top: sensor equipped tool holder A and bottom: multi component dynamometer with simulation for $a_e = 25\,\mathrm{mm}$, $f_z = 0.05\,\mathrm{mm}$, $a_\mathrm{p} = 3\,\mathrm{mm}$ and $v_c = 220\,\mathrm{m/min}$

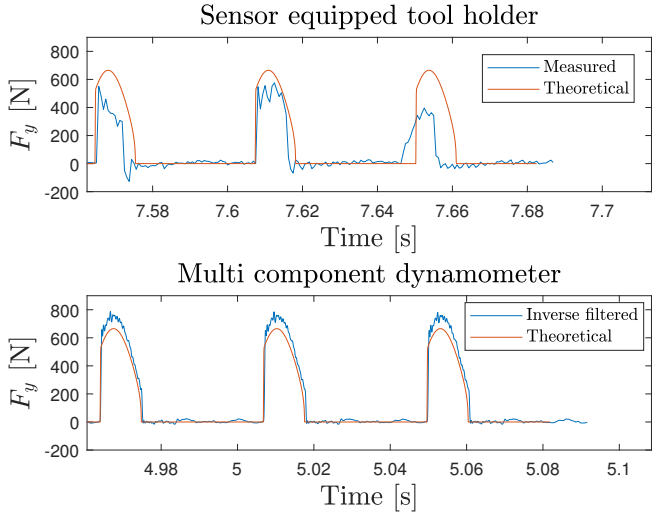

Figure 4.20: Comparison of F_y for top: sensor equipped tool holder A and bottom: multi component dynamometer with simulation for $a_e = 25\,\mathrm{mm}$, $f_z = 0.05\,\mathrm{mm}$, $a_\mathrm{p} = 3\,\mathrm{mm}$ and $v_c = 220\,\mathrm{m/min}$

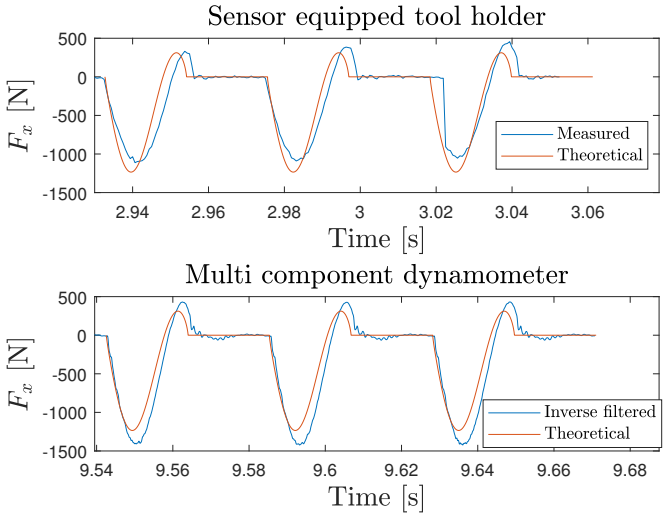

Figure 4.21: Comparison of F_x for top: sensor equipped tool holder A and bottom: multi component dynamometer with simulation for $a_e = 50\,\mathrm{mm}$, $f_z = 0.15\,\mathrm{mm}$, $a_\mathrm{p} = 3\,\mathrm{mm}$ and $v_c = 220\,\mathrm{m/min}$

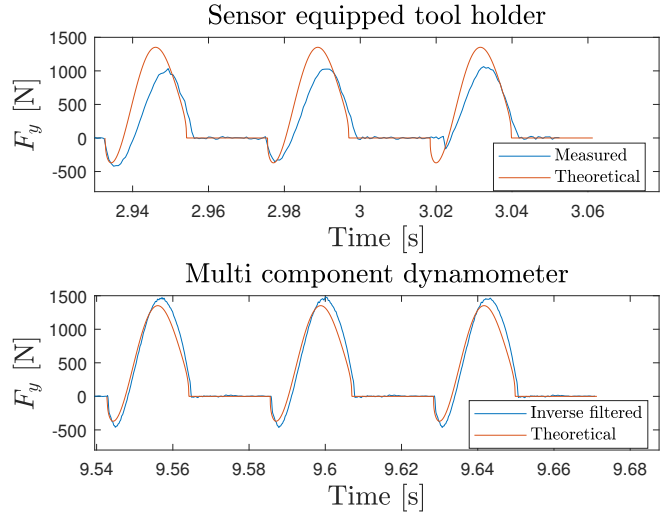

Figure 4.22: Comparison of F_y for top: sensor equipped tool holder A and bottom: multi component dynamometer with simulation for $a_e = 50\,\mathrm{mm}$, $f_z = 0.15\,\mathrm{mm}$, $a_\mathrm{p} = 3\,\mathrm{mm}$ and $v_c = 220\,\mathrm{m/min}$

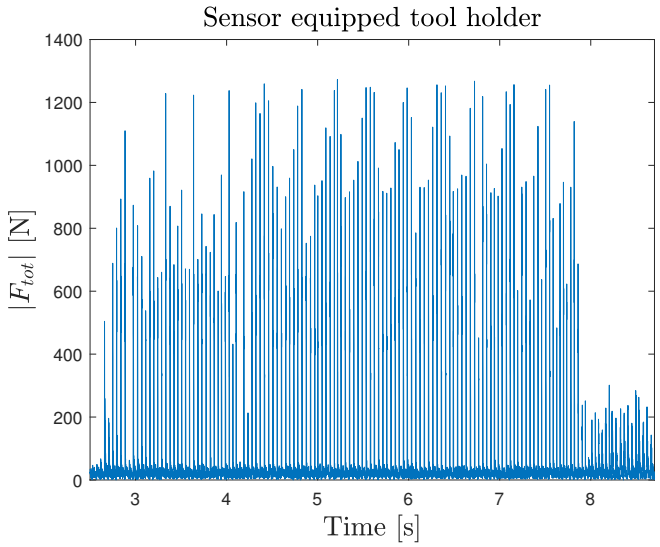

Figure 4.23: $|F_{tot}|$ acquired from sensor equipped tool holder A for $a_e = 5\,\mathrm{mm}$, $f_z = 0.15\,\mathrm{mm}$, $a_\mathrm{p} = 3\,\mathrm{mm}$ and $v_c = 220\,\mathrm{m/min}$

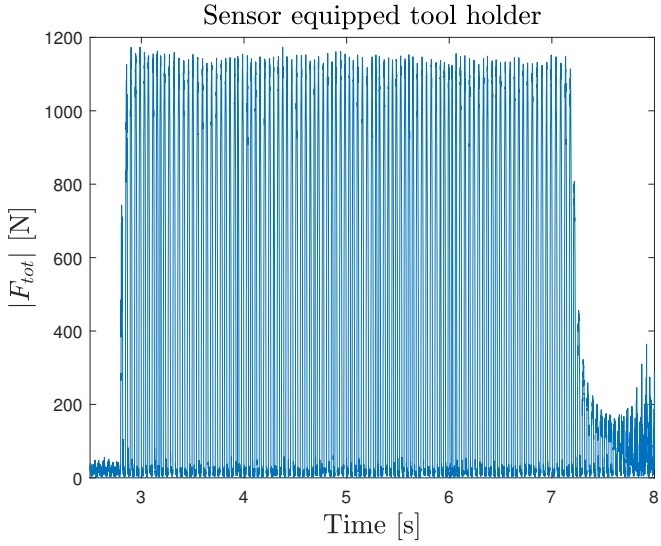

Figure 4.24: $|F_{tot}|$ acquired from sensor equipped tool holder A for $a_e = 50\,\mathrm{mm}$, $f_z = 0.15\,\mathrm{mm}$, $a_\mathrm{p} = 3\,\mathrm{mm}$ and $v_c = 220\,\mathrm{m/min}$

Sensor equipped tool holder B

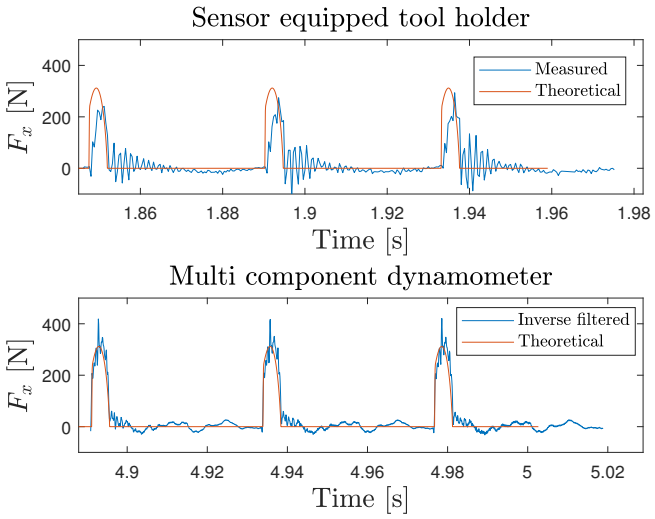

Figure 4.25: Comparison of F_x for top: sensor equipped tool holder B and bottom: multi component dynamometer with simulation for $a_e = 5\,\mathrm{mm}$, $f_z = 0.15\,\mathrm{mm}$, $a_\mathrm{p} = 3\,\mathrm{mm}$ and $v_c = 220\,\mathrm{m/min}$

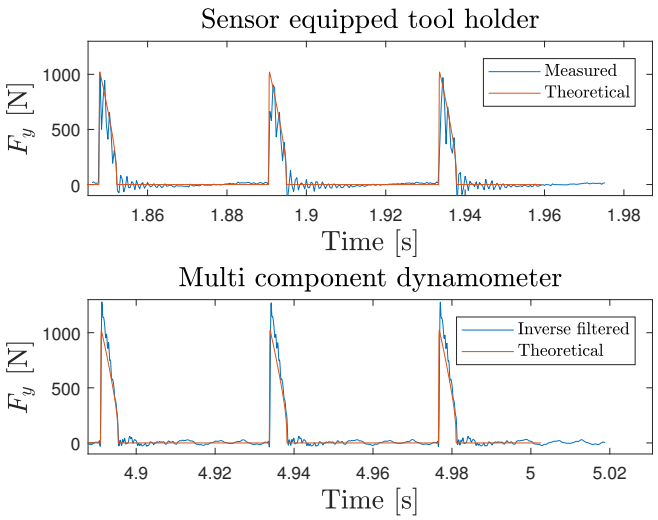

Figure 4.26: Comparison of F_y for top: sensor equipped tool holder B and bottom: multi component dynamometer with simulation for $a_e = 5\,\mathrm{mm}$, $f_z = 0.15\,\mathrm{mm}$, $a_\mathrm{p} = 3\,\mathrm{mm}$ and $v_c = 220\,\mathrm{m/min}$

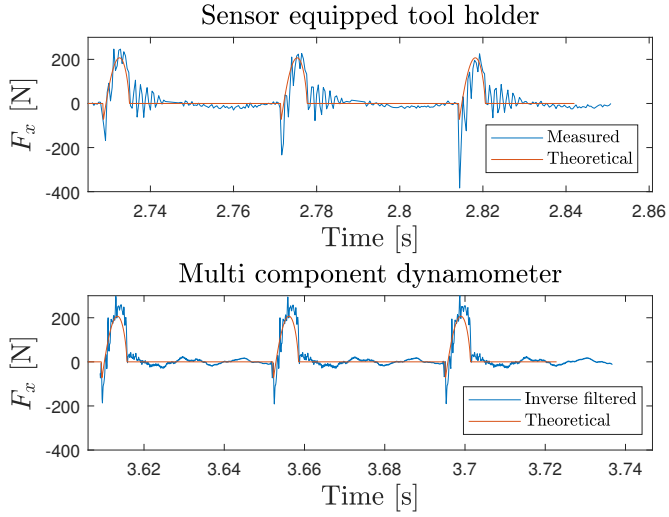

Figure 4.27: Comparison of F_x for top: sensor equipped tool holder B and bottom: multi component dynamometer with simulation for $a_e = 10\,\mathrm{mm}$, $f_z = 0.1\,\mathrm{mm}$, $a_\mathrm{p} = 3\,\mathrm{mm}$ and $v_c = 220\,\mathrm{m/min}$

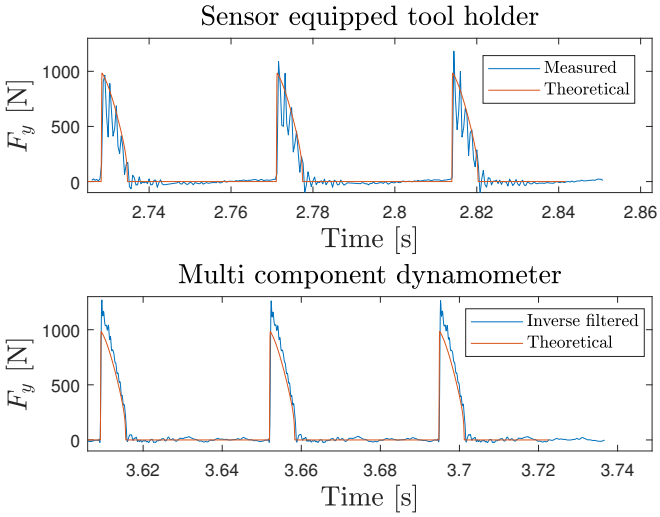

Figure 4.28: Comparison of F_y for top: sensor equipped tool holder B and bottom: multi component dynamometer with simulation for $a_e = 10\,\mathrm{mm}$, $f_z = 0.1\,\mathrm{mm}$, $a_\mathrm{p} = 3\,\mathrm{mm}$ and $v_c = 220\,\mathrm{m/min}$

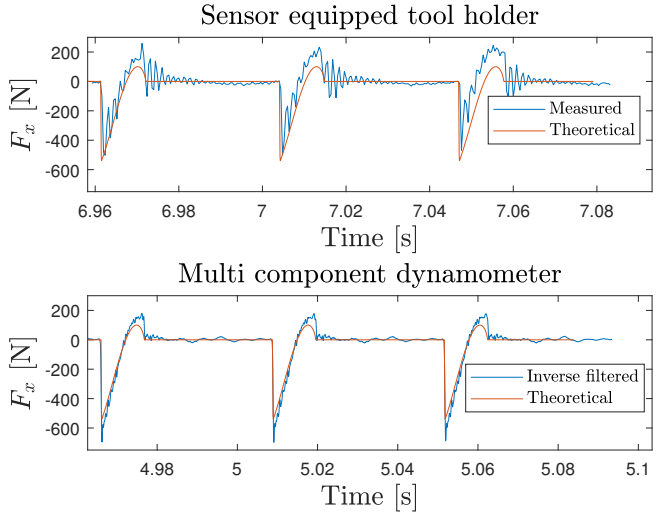

Figure 4.29: Comparison of F_x for top: sensor equipped tool holder B and bottom: multi component dynamometer with simulation for $a_e = 25\,\mathrm{mm}$, $f_z = 0.05\,\mathrm{mm}$, $a_\mathrm{p} = 3\,\mathrm{mm}$ and $v_c = 220\,\mathrm{m/min}$

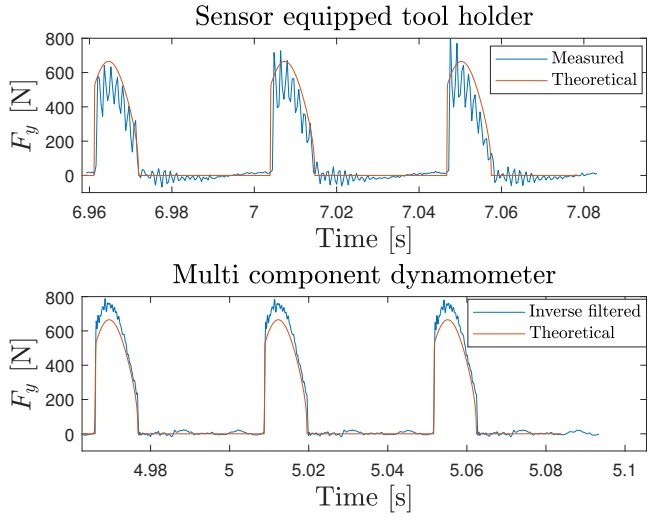

Figure 4.30: Comparison of F_y for top: sensor equipped tool holder B and bottom: multi component dynamometer with simulation for $a_e = 25\,\mathrm{mm}$, $f_z = 0.05\,\mathrm{mm}$, $a_\mathrm{p} = 3\,\mathrm{mm}$ and $v_c = 220\,\mathrm{m/min}$

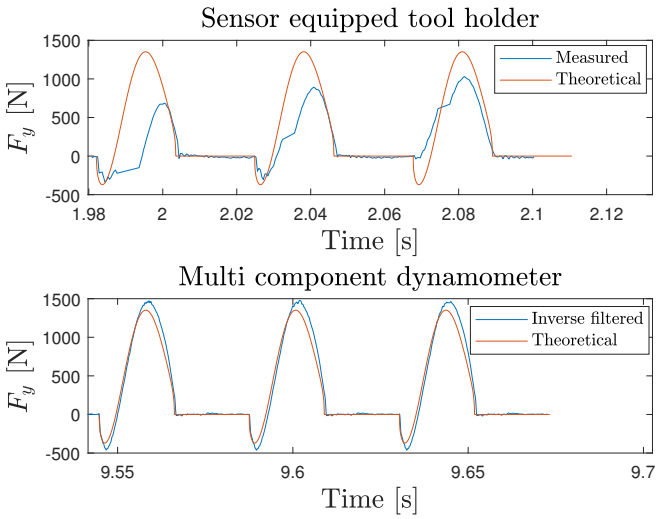

Figure 4.31: Comparison of F_x for top: sensor equipped tool holder B and bottom: multi component dynamometer with simulation for $a_e = 50\,\mathrm{mm}$, $f_z = 0.15\,\mathrm{mm}$, $a_\mathrm{p} = 3\,\mathrm{mm}$ and $v_c = 220\,\mathrm{m/min}$

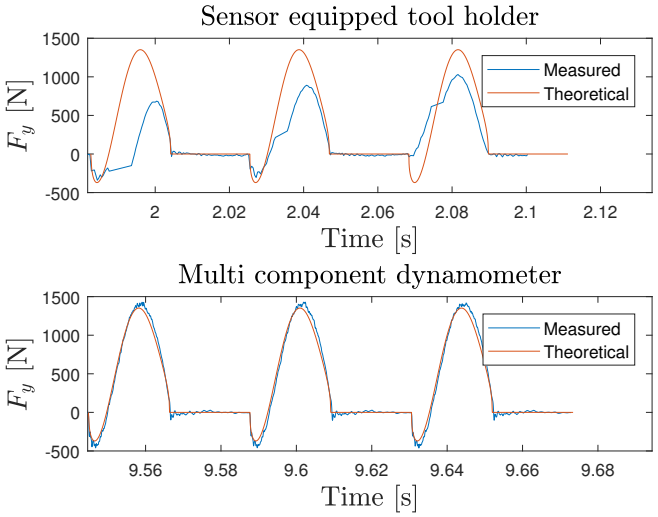

Figure 4.32: Comparison of F_y for top: sensor equipped tool holder B and bottom: multi component dynamometer with simulation for $a_e = 50\,\mathrm{mm}$, $f_z = 0.15\,\mathrm{mm}$, $a_\mathrm{p} = 3\,\mathrm{mm}$ and $v_c = 220\,\mathrm{m/min}$

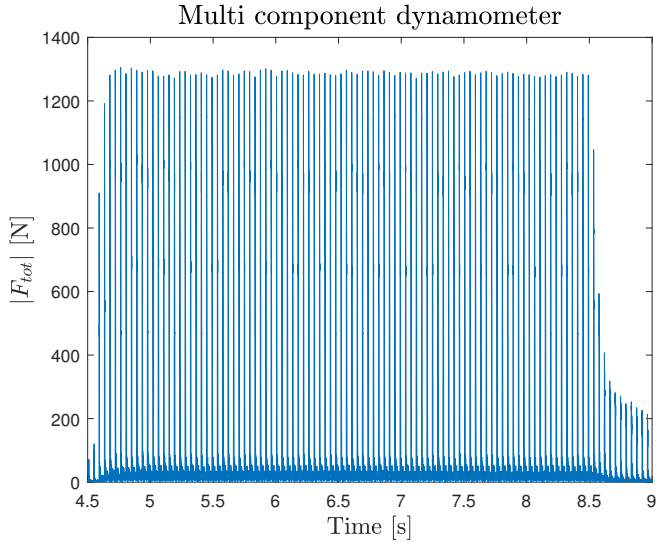

Figure 4.33: $|F_{tot}|$ acquired from multi component dynamometer for $a_e = 5\,\mathrm{mm}$, $f_z = 0.15\,\mathrm{mm}$, $a_\mathrm{p} = 3\,\mathrm{mm}$ and $v_c = 220\,\mathrm{m/min}$

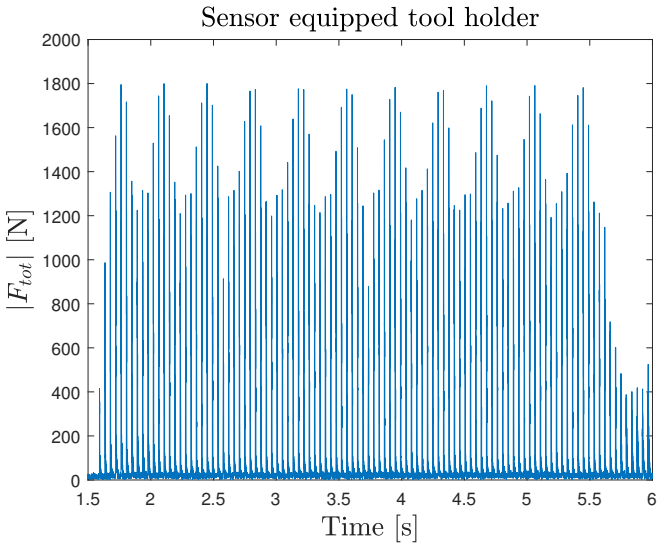

Figure 4.34: $|F_{tot}|$ acquired from sensor equipped tool holder B for $a_e = 5\,\mathrm{mm}$, $f_z = 0.15\,\mathrm{mm}$, $a_\mathrm{p} = 3\,\mathrm{mm}$ and $v_c = 220\,\mathrm{m/min}$

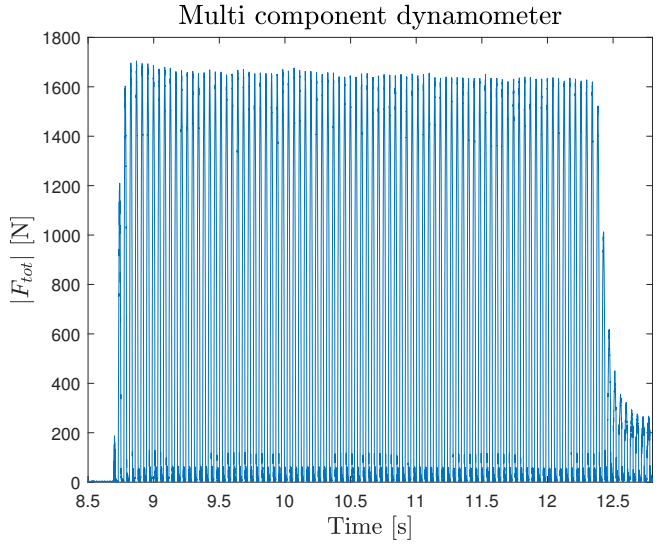

Figure 4.35: $|F_{tot}|$ acquired from multi component dynamometer for $a_e = 50\,\mathrm{mm}$, $f_z = 0.15\,\mathrm{mm}$, $a_\mathrm{p} = 3\,\mathrm{mm}$ and $v_c = 220\,\mathrm{m/min}$

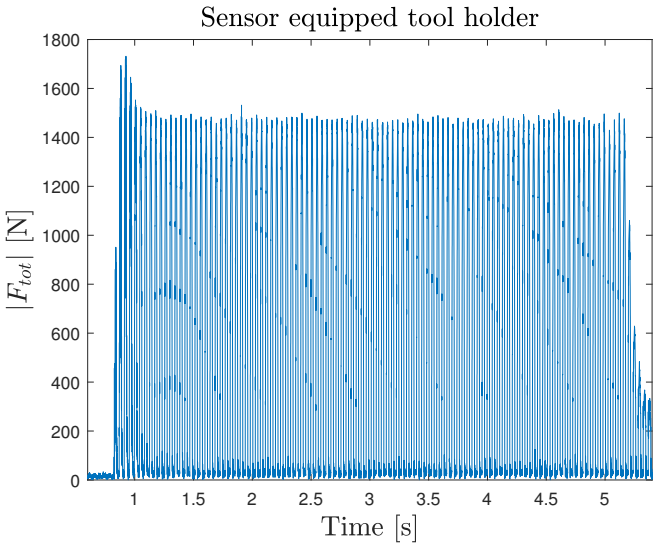

Figure 4.36: $|F_{tot}|$ acquired from sensor equipped tool holder B for $a_e = 50\,\mathrm{mm}$, $f_z = 0.15\,\mathrm{mm}$, $a_\mathrm{p} = 3\,\mathrm{mm}$ and $v_c = 220\,\mathrm{m/min}$

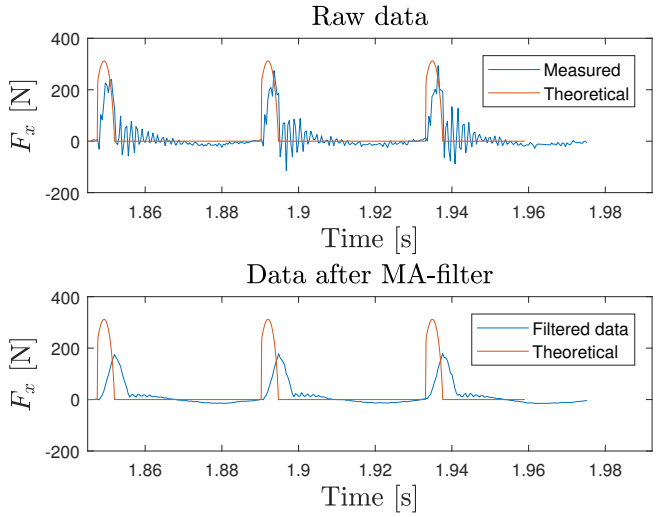

Figure 4.37: MA-filter of length 10 applied on data acquired from sensor equipped tool holder B for $a_e = 5\,\mathrm{mm}$, $f_z = 0.15\,\mathrm{mm}$, $a_\mathrm{p} = 3\,\mathrm{mm}$ and $v_c = 220\,\mathrm{m/min}$

4.4.2 Drilling

Figures 4.39, 4.40, 4.43, and 4.44 shows the raw measurement data of axial force, F_z, for the drilling operations that were conducted. Due to the use of a symmetrical drill, figure 4.38, the force components in $x-$ and $y-$ direction cancels each other out in the multi component dynamometer. Both the methods of measuring axial force yields similar results, with the sensor equipped tool holder having a higher noise level; $\pm 150\,\mathrm{N}$ according to the manufacturer. The proposed solution by the manufacturer is to use a MA filter of length 1 to 100, which also is their proposed filter for milling. In figures 4.41, 4.42, 4.45, and 4.46 the torque for the drilling operations is shown. The tables 4.3 and 4.4 shows the standard deviation of the noise and the mean value during engagement for both torque and F_z in the respective drilling measurement. In the drilling tests both a stationary and rotating multi component dynamometer were used as references and the stationary multi component was used for measuring F_z and the rotating for measuring torque.

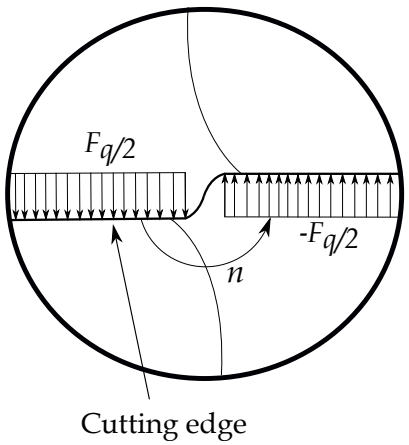

Figure 4.38: Example of top view on a symmetrical drill

Sensor equipped tool holder A

Due to the sampling problem mentioned in subsection 4.4.1 the time stamps for each sample in the drilling measurements were recalculated for sensor equipped tool holder A.

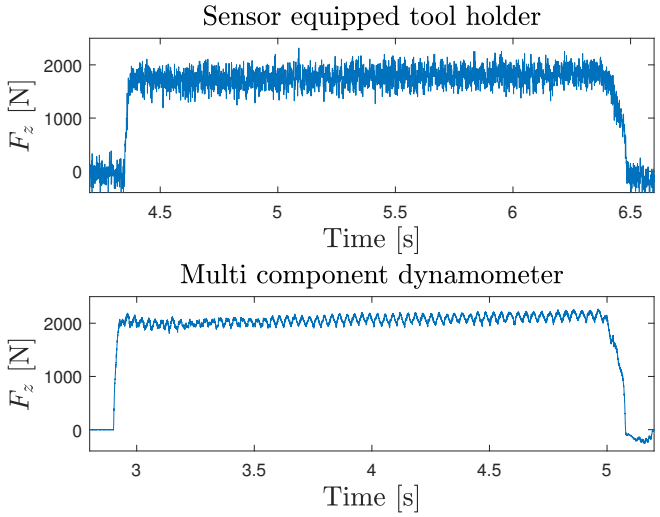

Figure 4.39: Comparison between sensor equipped tool holder A and stationary multi component dynamometer, F_z for $v_c = 80\,\mathrm{m/min}$ and $f_n = 0.2\,\mathrm{mm}$

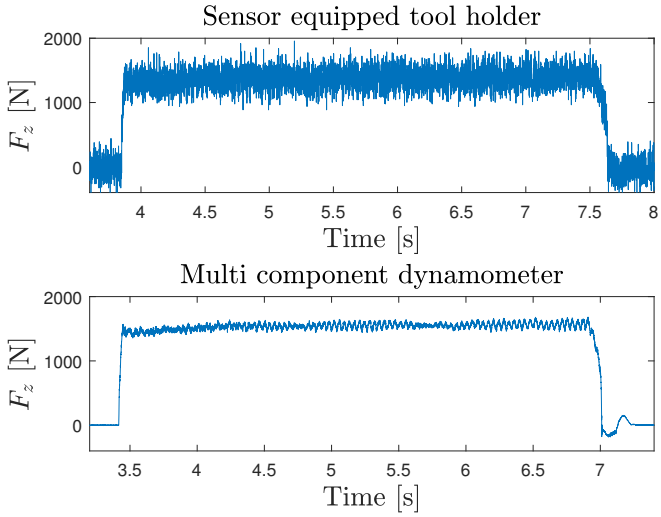

Figure 4.40: Comparison between sensor equipped tool holder A and stationary multi component dynamometer, F_z for $v_c = 80\,\mathrm{m/min}$ and $f_n = 0.12\,\mathrm{mm}$

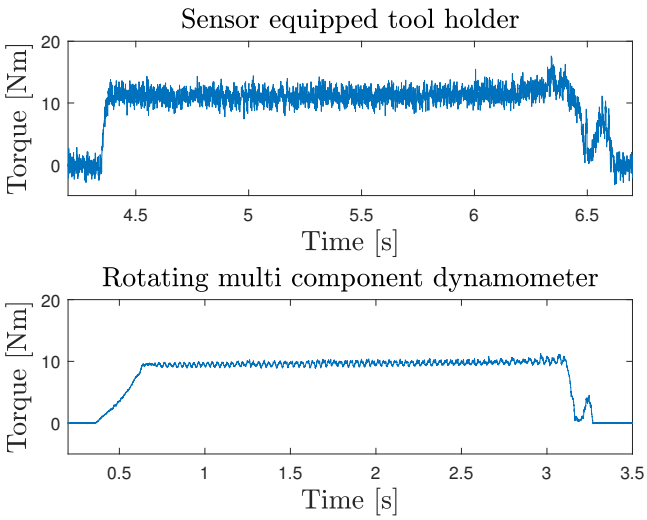

Figure 4.41: Comparison between sensor equipped tool holder A and rotating multi component dynamometer, torque for $v_c = 80\,\mathrm{m/min}$ and $f_n = 0.2\,\mathrm{mm}$

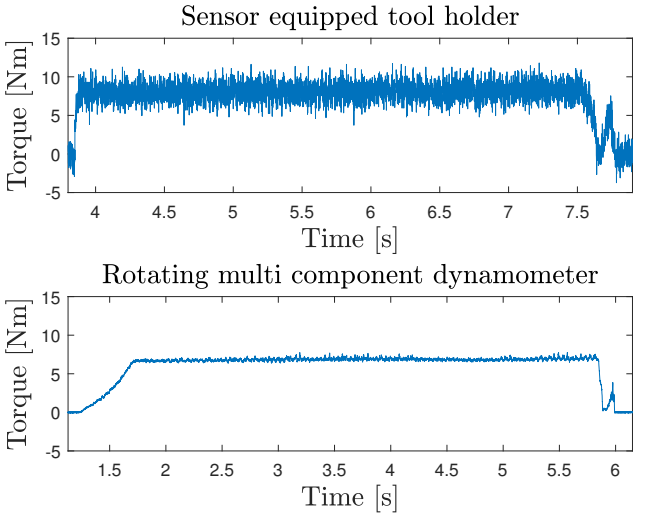

Figure 4.42: Comparison between sensor equipped tool holder A and rotating multi component dynamometer, torque for $v_c = 80\,\mathrm{m/min}$ and $f_n = 0.12\,\mathrm{mm}$

Sensor equipped tool holder B

The sensor equipped tool holder B had the same sampling frequency as specified hence no modification of the time stamps was needed.

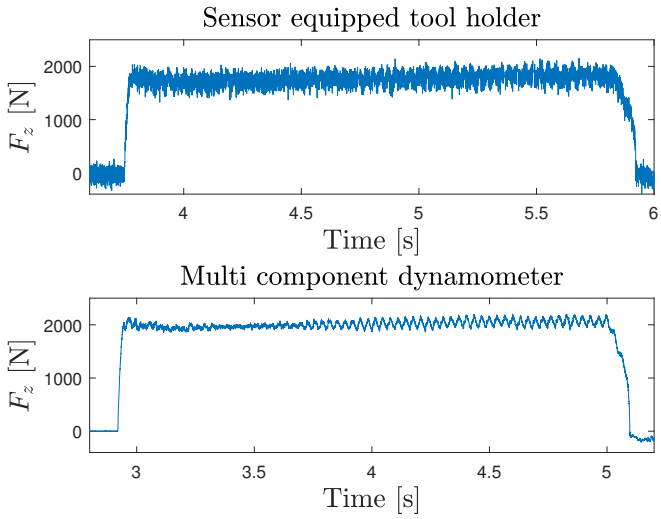

Figure 4.43: Comparison between sensor equipped tool holder B and stationary multi component dynamometer, F_z for $v_c = 80\,\mathrm{m/min}$ and $f_n = 0.2\,\mathrm{mm}$

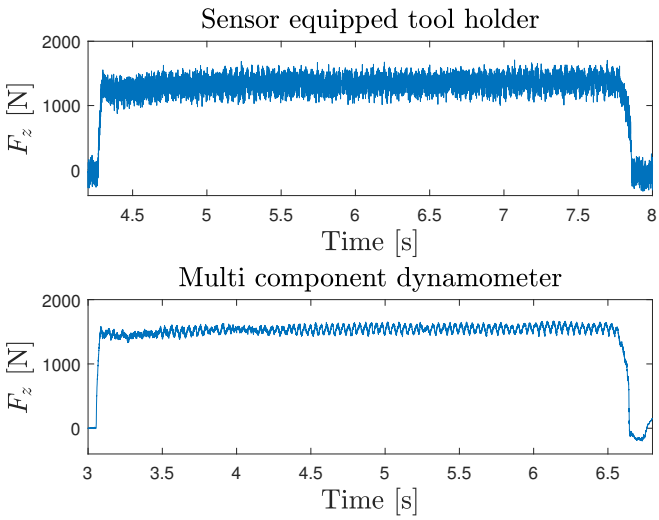

Figure 4.44: Comparison between sensor equipped tool holder B and stationary multi component dynamometer, F_z for $v_c = 80\,\mathrm{m/min}$ and $f_n = 0.12\,\mathrm{mm}$

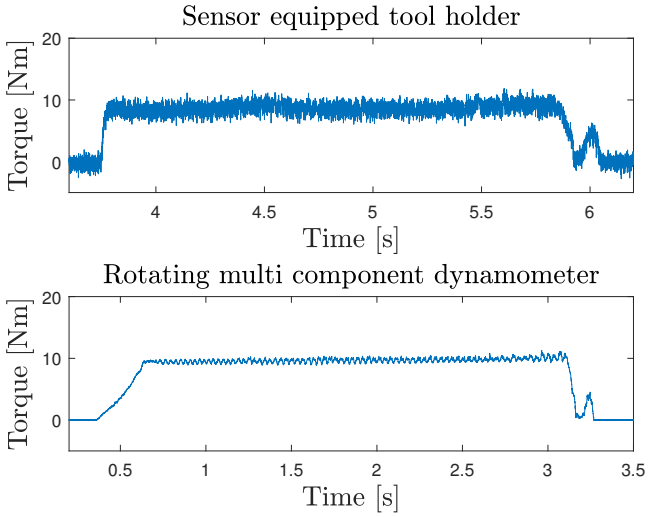

Figure 4.45: Comparison between sensor equipped tool holder B and rotating multi component dynamometer, torque for $v_c = 80\,\mathrm{m/min}$ and $f_n = 0.2\,\mathrm{mm}$

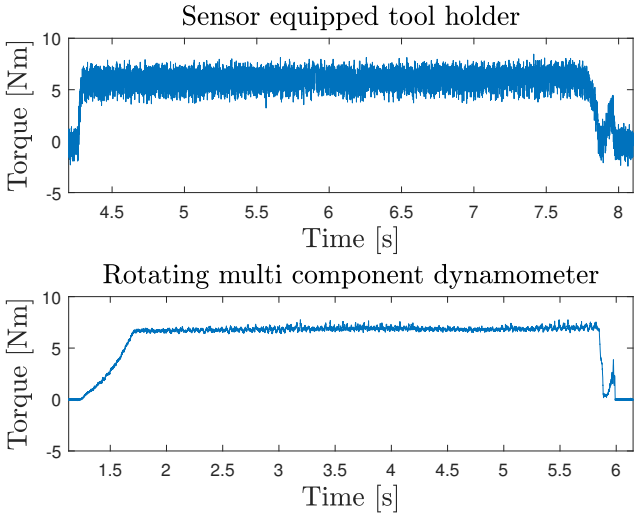

Figure 4.46: Comparison between sensor equipped tool holder B and rotating multi component dynamometer, torque for $v_c = 80\,\mathrm{m/min}$ and $f_n = 0.12\,\mathrm{mm}$

	Tool holder A	Tool holder B	Stationary dynamometer	Rotating dynamometer
σ_{Torque}	1.01 N m	0.76 N m	-	0.04 N m
σ_{F_z}	135.65 N	104.28 N	1.30 N	4.09 N
μ_{Torque}	11.11 N m	8.89 N m	-	9.66 N m
μ_{F_z}	1539.11 N	1909.80 N	2092.86 N	2066.79 N

Table 4.3: Standard deviation and mean for drilling measurements with $v_c = 80\,\mathrm{m/min}$ and $f_n = 0.2$. Torque was not measured with the stationary multi component dynamometer hence it is not shown.

	Tool holder A	Tool holder B	Stationary dynamometer	Rotating dynamometer
σ_{Torque}	1.01 N m	0.77 N m	-	0.04 N m
σ_{F_z}	143.81 N	102.58 N	1.31 N	3.82 N
μ_{Torque}	8.07 N m	6.23 N m	-	6.87 N m
μ_{F_z}	1449.84 N	1380.05 N	1547.44 N	1513.79 N

Table 4.4: Standard deviation and mean for drilling measurements with $v_c = 80\,\text{m/min}$ and $f_n = 0.12$. Torque was not measured with the stationary multi component dynamometer hence it is not shown.

Figure 4.47 shows an example of how the data may look after a Butterworth and MA-filter is applied, the normalized cut off-frequency was set to $f_c = 0.1$ where 1 is the Nyquist-frequency, $\frac{f_s}{2}$. Table 4.5 shows the standard deviation of the noise, which has been significantly reduced. The cut off-frequency for the MA-filter was calculated as. Given a MA filter of length N it has the amplitude response

$$|H(\omega)| = \frac{1}{N} \cdot \left| \frac{\sin \frac{\omega N}{2}}{\sin \frac{\omega}{2}} \right| \tag{4.1}$$

which for $f_c = 0.1$ yielded that $N \approx 9$.

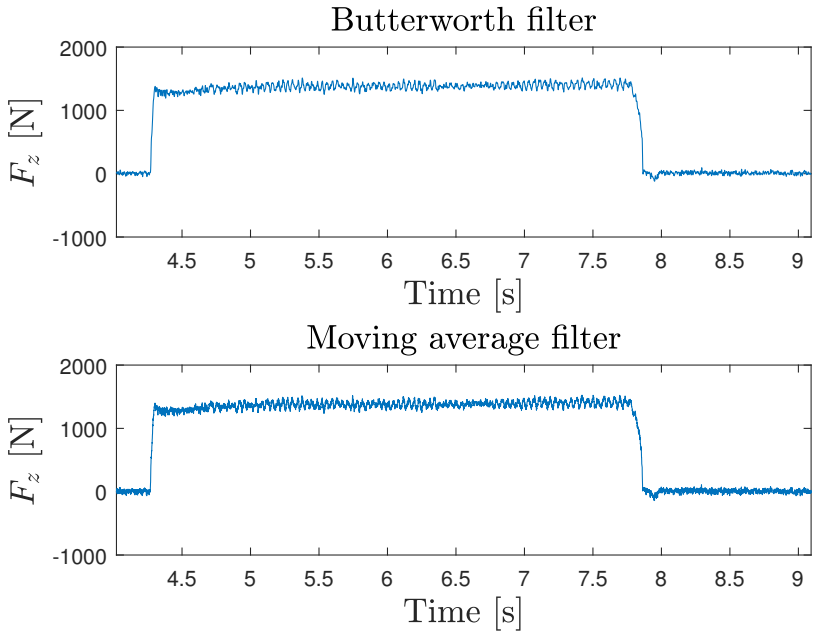

Figure 4.47: Data from sensor equipped tool holder B after different low pass-filter with normalised $f_c = 0.1$

	Butterworth filter	MA-filter
σ_{Fz}	18.11 N	22.53 N

Table 4.5: Standard deviation of noise after filter

Chapter 5
Evaluation and Conclusion

The evaluation of the work presented in this thesis is divided into three parts: dynamic behaviour, performance of inverse filter, and sensor equipped tool holders performance. This to make a distinct separation of the evaluations since they are based on different measurements and results. Even though the inverse filter was used when comparing the sensor equipped tool holders with the multi component dynamometer, the process to obtain the inverse filter and evaluating it was separated from the evaluation of the sensor equipped tool holders. The evaluation covers the possibilities and limitations of the obtained inverse filter and the sensor equipped tool holders.

5.1 Change in dynamic behaviour

An analysis of the results, in table 4.1 and 4.2, from the dynamic testing shows that the dynamic stiffness increases by the mounting of the sensor. This is due to the mounting of the sensor ring on the outside of the tool holder structure. Although the sensor-system increases stiffness, due to its mounting, figure 3.1, it impairs the accessibility of the tool holder. Meaning that depending on the workpiece, using the sensor equipped tool holders makes certain cutting operations impossible. The reason that the sensor-system stiffens tool holder B more than A, is thought to be that the original design of tool holder B is straight compared to tool holder A which has a cone like-shape. The more slender design is impairing tool holder B from a machining stability perspective and is therefor more susceptible for the increased stiffness caused by the sensor system.

5.2 Inverse filter

The filter obtained to remove the multi component dynamometers dynamic influence from cutting force measurements was successfully implemented during this thesis. Comparing the method of using an inverse filter and low pass-filter at 2000 Hz, with the current method of just a low pass-filter at 250 Hz, yields that there is less signal distortion. Comparing the inverse filter-method with raw data it can be seen that the inverse filter-method successfully reduces the amount of

signal distortion due to dynamic influence yet preserves the distinct response at tool engagement entry.

As mentioned in chapter 4 the filter in x-direction was more sensitive to noise, compared to the $y-$direction. The reason for this might be that at 3030 Hz there is dip in FRF of the multi component dynamometer, figure 4.2a. This led to that the inverse filter had a high amplification at this frequency and if there was any noise present at this frequency it was amplified.

Another aspect that is of importance when applying an obtained inverse filter is that the data that is filtered has the same sampling frequency as the measurement of the multi component dynamometer FRFs, otherwise the filter will not work as intended. In this thesis this was solved by down-sampling the raw data from the multi component dynamometer from its original sample rate of 19 200 Hz to 12 000 Hz. This was achieved by interpolating the measured raw data using the desired number of sample points. This did not lead to any noticeable loss of crucial information.

Here it should strongly be emphasised that the inverse filter is dependent on the workpiece mounted on the multi component dynamometer. This means that the filter obtained in this thesis will not work as intended if applied on a measurement with the same multi component dynamometer with a different workpiece. Also the machine tool where the multi component force dynamometer is mounted affects its dynamic properties, and thereby the FRFs. Due to this it is not possible to have one filter that works for all setups of the multi component dynamometer. It is however possible to standardise the procedure of the cutting force measurements in such way that during the mounting of the workpiece a measurement of the FRF is performed. Given the FRF the calculation of an inverse filter, and re-sampling of the cutting force signal can be done automatically.

5.3 Sensor equipped tool holders

As said in subsection 4.4.1 the actual sampling frequency was not the same as the saved measurement files indicated for the sensor equipped tool holder A. This was first noticed when calculating RPM for the milling tests. The sampling frequency according to the measurement data was 2500 Hz, the frequency according to the documentation was 1600 Hz. Conformation of a difference between the sampling rates was performed by checking that

$$T \cdot f_s = S_n \tag{5.1}$$

held true, where T is the measurement time, in seconds, f_s the specified sampling frequency, and S_n the number of samples collected. Equation 5.1 held true for both the multi component dynamometer and the sensor equipped tool holder B,

while it did not for the sensor equipped tool holder A. Here it should be emphasised that the sampling frequency was calculated using the time stamps in the saved data files from the measurements, which eliminates the possibility of a setting being wrong. For both sensor equipped tool holders the time between each sample was 0.0004 s, according to each of the saved data files. However, the actual time between each sample for sensor equipped tool holder A was 0.000 571 second to 0.000 625 second.

5.3.1 Milling tests

As seen in the figures displaying extracts of all cutting force measurements for the milling tests, the sensor equipped tool holders performance is not as good as the multi component dynamometer or the theoretical simulations in terms of accuracy, consistency and periodicity. In figures 4.17, 4.18, 4.19, and 4.20 it is seen that the issue with sampling frequency for sensor equipped tool holder A causes the time between engagements to vary; this should not be the case. Overlooking this it can be seen that both sensor equipped tool holder seems to have similar problems with consistency. The issue with consistency can clearly be seen in figure 4.32, where it on the third peak does not capture the decline in F_y and in the first two peaks there is a case of package loss during the engagement. This is however a problem with the wireless communication, and not with the sensors them self.

Comparing figure 4.33 with figure 4.34 and 4.23 it is seen that the sensor equipped tool holders fails to capture all force peaks correctly. All peaks in total cutting force should have similar peak value, since the peaks represents identical cutting engagements. This is most likely due to the sampling frequency of the sensor equipped tool holder, this since it does not have the same behaviour for larger a_e as in figures 4.36 and 4.24 or in the drilling tests; where high sampling rate is not as crucial. Comparing figure 4.23 and 4.34 the issue with varying sampling rate for the sensor equipped tool holder A is seen. As the varying amplitude on the force peaks is periodic in figure 4.34 where the sampling frequency is constant, while it is not as periodic in figure 4.23 where the sampling frequency varies. F_{tot} is calculated as

$$F_{\text{tot}} = \sqrt{F_{\text{x}}^2 + F_{\text{y}}^2} \tag{5.2}$$

for the multi component dynamometer, and as

$$F_{\text{tot}} = \sqrt{F_{\text{r}}^2 + F_{\text{t}}^2} \tag{5.3}$$

for the sensor equipped tool holders. The use of different coordinate systems do not affect the absolute value of the cutting force. It should be pointed out that using cutting speeds larger than $v_c = 220\,\text{m/min}$ would result in higher spindle speeds, which for small a_e would decrease the accuracy of the sensor equipped tool holders. This since a higher spindle speed would lead to that every cutting engagement frequency would increase, thus decreasing the number of samples per

engagement and thereby the accuracy and consistency.

5.3.2 Drilling tests

On the drilling tests, the sensor equipped tool holders performance is more consistent. Since high sampling rate is not as important in drilling as it is in milling, the sensor equipped tool holder does not miss events as it does in figure example 4.32. The noise that is apparent in figure 4.39-4.46, standard deviation of the noise is shown in table 4.3, for the sensor equipped tool holder can be reduced by low pass-filtering, either a butterworth-filter or, as suggested by the manufacturer, a MA-filter. Usage of a MA-filter on a milling operation is seen in figure 4.37, as seen this filtering method distorts the signal for short milling engagements and hence is it not to recommend. The length of the filter was 10 samples, using an even longer MA-filter would distort the signal more. Comparing the effect of a MA-filter on a drilling measurement, figure 4.47, with the effect on milling measurements, figure 4.37, it is seen that MA-filters is more suitable for drilling applications since there is less distortions. Table 4.5 shows the noise level, which has been reduced, with use of low pass-filter. The reason for the higher noise level in F_z compared to the torque, table 4.3 and 4.4, is most likely due to the calibration values of the strain gauges being significantly larger, table 2.2, in this direction.

Chapter 6
Discussion and future work

The discussion in this section covers what could have been done to improve the evaluation and measurements. Due to time frames and limitations in measurements equipment, it was not possible to achieve ideal measurement conditions. Regarding sensor equipped tool holders there are some suggestions on what need to be adjusted if they are to be considered a reliable tool in cutting process evaluations. Concerning the use of inverse filtering to enhance quality of cutting force measurements, recommendations of how to implement this method are presented.

6.1 Error sources

A potential source of uncertainty was the limited access to computers during the milling and drilling measurements. Due to this the cutting operation was hence performed sequentially; once for the sensor equipped tool holder and once for the multi component dynamometer. Although the cutting parameters, CNC-machine, tool, and cutting data was the same, having the two measurements system measure simultaneously on the same cutting operation would have been ideal. The probability of the two measurement systems interfering with each other is considered negligible.

As previously mentioned, the sensor equipped tool holder measure bending moment and not force, however the force could be calculated if the lever arm was known. This lever arm was measured using calipers, this could cause the length of the lever arm to not be accurate to the true value. However, this would only affect the amplitude of the signal, and not its dynamic behaviour, for example as in figure 4.25.

For the drilling measurements, the tests with the rotating multi component dynamometer were performed on a different CNC-machine than the tests with the sensor equipped tool holders. This since the rotating multi component dynamometer could not be mounted in the same machine tool as where the other tests were performed. Both the cutting parameters and the tool were the same, which should make the effect of having used two different CNC-machines negligible. In figure 4.45 and 4.46 torque has a lower gradient in the beginning of the engagement

for the rotating multi component dynamometer compared to the sensor equipped tool holder and stationary multi component dynamometer. This is because a hole was pre-drilled before the measurement with the sensor equipped tool holder and stationary multi component dynamometer. Due the shape of the drill, see figure 6.1, if there is a pre-drilled hole the entire cutting edges of the drill will come in contact with the workpiece directly and therefore resulting in a quick rise as in figure 4.44.

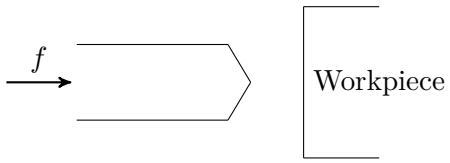

Figure 6.1: Example of side view of drill

6.1.1 Sampling frequency

As mentioned in subsection 4.4.1, the sampling frequency was not the same as the specified. Knowing the cutting parameters for the milling operations performed, the true sample frequency could be calculated. For all tests $n = 1400\,\text{rev/min}$, which for a sample rate of $f_s = 2500\,\text{samples/s}$ would be 107 samples between the engagements. This was the case for sensor equipped tool holder B, while it for sensor equipped tool holder A was either 67 samples and 75 samples between each engagement. Indicating a sample frequency alternating between 1600 Hz and 1750 Hz during the measurement. In figures 4.15-4.22 the time stamps was recalculated using $f_s = 1600\,\text{Hz}$, which is why the time between the cutting engagements sometimes varies. Even though the time stamps may not be correct, the accuracy and consistency of sensor equipped tool holder A was still evaluated.

6.1.2 Wireless communication

The wireless communication in the sensor equipped tool holders sends data in packages of seven samples. The sensor equipped tool holder saves seven samples of data, time, tension, torque, bending moment x, and bending moment y, before the package is sent to the receiver.

Figure 6.2 shows an example of a case of packet loss during a milling operation. The peak at 4.7 second is missing. Due to loss of a packet during the engagement the peak is absent for both the bending moment and torque, this is also the case for tension for this measurement. The reason for these kind of losses can be many, although one of the most likely cases during the measurements performed for this thesis is that someone outside the machine tool or something inside the machine tool was blocking the signal. This reason is likely because the machine operator being positioned between the sensor equipped tool holder and the radio receiver and the fixture and spindle is moving inside the machine tool during machining.

It should also be noticed that the wireless communication between the sensor equipped tool holders and radio receiver is in the 2.4 GHz frequency band, which is unlicensed and therefore crowded [23]. Having much interference in the channel used for communication may increase the risk of packet loss. The channel used for communication can be changed if needed.

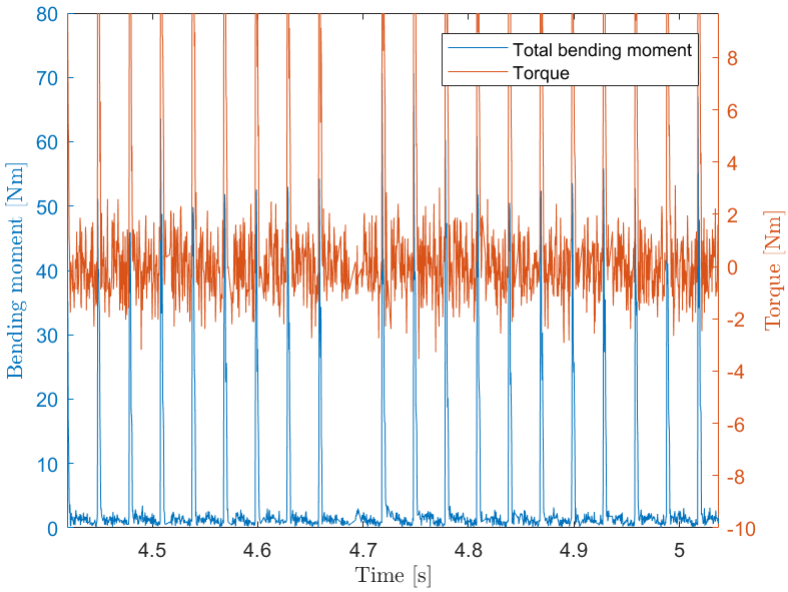

Figure 6.2: Example of packet loss during a cutting engagement

6.2 Future work

As said in chapter 5, the sensor equipped tool holders requires a considerable increase in sampling frequency. If the sensor equipped tool holder should be suitable for general milling applications it is to be recommended that sampling frequency should be at least 10 kHz. If the sensor equipped tool holders are to be used for direct feedback to the machine tool, a more robust communication protocol is necessary.

In order to make reduction of dynamic influence a method that is practically applicable at AB Sandvik Coromant, knowledge on how dynamic influence distort measurement data must be increased. Then since a new filter is needed for each measurement, a standardised procedure of obtaining an inverse filter is required.

Bibliography

[1] Jay F. Tu. "Strain field analysis and sensor design for monitoring machine tool spindle bearing force". In: *International Journal of Machine Tools and Manufacture* 36 (2 1996), pp. 203–216.

[2] S.C. Lin and R.J. Lin. "Tool wear monitoring in face milling using force signals". In: *Wear* 198.1 (1996), pp. 136–142. ISSN: 0043-1648. DOI: https://doi.org/10.1016/0043-1648(96)06944-X. URL: http://www.sciencedirect.com/science/article/pii/004316489606944X.

[3] M.Santochi G.Dini G.Tantussi M.Beghini. "A Sensor-Integrated Tool for Cutting Force Monitoring". In: *CIRP Annals* 46 (1 1997), pp. 49–52.

[4] Christopher A Suprock and Jeffery S. Nichols. "A low cost wireless high bandwidth transmitter for sensor-integrated metal cutting tools and process monitoring". In: *Int. J. Mechatronics and Manufacturing Systems* 2 (July 2009).

[5] Simon S. Park. "High frequency bandwidth cutting force measurements in milling using the spindle integrated force sensor system". PhD thesis. 2003. DOI: http://dx.doi.org/10.14288/1.0081000. URL: https://open.library.ubc.ca/cIRcle/collections/831/items/1.0081000.

[6] Qiaokang Liang et al. "Design and Analysis of a Sensor System for Cutting Force Measurement in Machining Processes". In: *Sensors* 16 (Jan. 2016), p. 70.

[7] Yusuf Altintas. *Manufacturing Automation: metal cutting mechanincs, machine tool vibrations, and CNC design*. Cambridge: Cambridge University Press, 2000.

[8] Kienzle O. “Die Bestimmung von Kräften und Leistungen an spanenden Werkzeugen und Werkzeugmaschinen”. In: *Zeitschrift des Vereins deutscher Ingenieure* (1952), pp. 657–662.

[9] Y. Altintaş and E. Budak. “Analytical Prediction of Stability Lobes in Milling”. In: *CIRP Annals* 44.1 (1995), pp. 357–362. ISSN: 0007-8506. DOI: https://doi.org/10.1016/S0007-8506(07)62342-7. URL: http://www.sciencedirect.com/science/article/pii/S0007850607623427.

[10] Anders Liljerehn. *Machine tool dynamics : a constrained state-space substructuring approach.* Doktorsavhandlingar vid Chalmers tekniska högskola. Ny serie: 4188. Göteborg : Chalmers University of Technology, 2016, 2016. ISBN: 9789175975078. URL: http://ludwig.lub.lu.se/login?url=http://search.ebscohost.com/login.aspx?direct=true&db=cat01310a&AN=lovisa.004950506&site=eds-live&scope=site.

[11] Erhan Budak and Yusuf Altintas. “Analytical Prediction of Chatter Stability in Milling—Part II: Application of the General Formulation to Common Milling Systems”. In: 120 (Mar. 1998).

[12] G. H. Gautschi. “Cutting Forces in Machining and Their Routine Measurement with Multi-Component Piezo-Electric Force Transducers”. In: *Proceedings of the Twelfth International Machine Tool Design and Research Conference*. Ed. by F. Koenigsberger and S. A. Tobias. London: Macmillan Education UK, 1972, pp. 113–120. ISBN: 978-1-349-01397-5. DOI: 10.1007/978-1-349-01397-5_15. URL: https://doi.org/10.1007/978-1-349-01397-5_15.

[13] V. Sharapov. *Piezoceramic Sensors. Microtechnology and MEMS*. Springer, 2011.

[14] Kistler. *Piezoelectric Theory*. https://www.kistler.com/?type=669&fid=92&model=download. Online; accessed 23 Mars 2018.

[15] John G. Proakis and Dimitris G. Manolakis. *Digital Signal Processing (3rd Ed.): Principles, Algorithms, and Applications*. Upper Saddle River, NJ, USA: Prentice-Hall, Inc., 1996. ISBN: 0-13-373762-4.

[16] Soo-Chang Pei and H.-S Lin. “Minimum-Phase FIR Filter Design Using Real Cepstrum”. In: 53 (Nov. 2006), pp. 1113–1117.

[17] Fredrik Gustafsson. “Determining the Initial States in Forward-Backward Filtering”. In: 44 (May 1996), pp. 988–992.

[18] Wazir Muhammad Laghari Mohammad Usman Baloch Muhammad Abid Mengal Syed Jalal Shah. "Performance Analysis of Analog Butterworth Low Pass Filter as Compared to Chebyshev Type-I Filter, Chebyshev Type-II Filter and Elliptical Filter". In: *Circuits and Systems* 5.9 (2014), pp. 209–216.

[19] E C. Levy. "Complex-Curve Fitting". In: AC-4 (May 1959), pp. 37–43.

[20] J.E. Dennis and R.B. Schnabel. *Numerical methods for unconstrained optimization and nonlinear equations*. Prentice-Hall series in computational mathematics. Prentice-Hall, 1983. ISBN: 9780136272168.

[21] Martin Magnevall et al. "High frequency measurements of cutting forces in milling by inverse filtering". In: *Machining Science and Technology* 16 (Dec. 2012).

[22] Min Wan, Wei Yin, and Wei-Hong Zhang. "Study on the Correction of Cutting Force Measurement with Table Dynamometer". In: *Procedia CIRP* 56 (2016). The 9th International Conference on Digital Enterprise Technology – Intelligent Manufacturing in the Knowledge Economy Era, pp. 119–123. ISSN: 2212-8271. DOI: https://doi.org/10.1016/j.procir.2016.10.035. URL: http://www.sciencedirect.com/science/article/pii/S2212827116310277.

[23] Matthew Loy Raju Karingattil Louis Williams. *ISM-Band and Short Range Device Regulatory Compliance Overview*. Tech. rep. 2005.

Appendices

Appendix A

Dynamic measurements

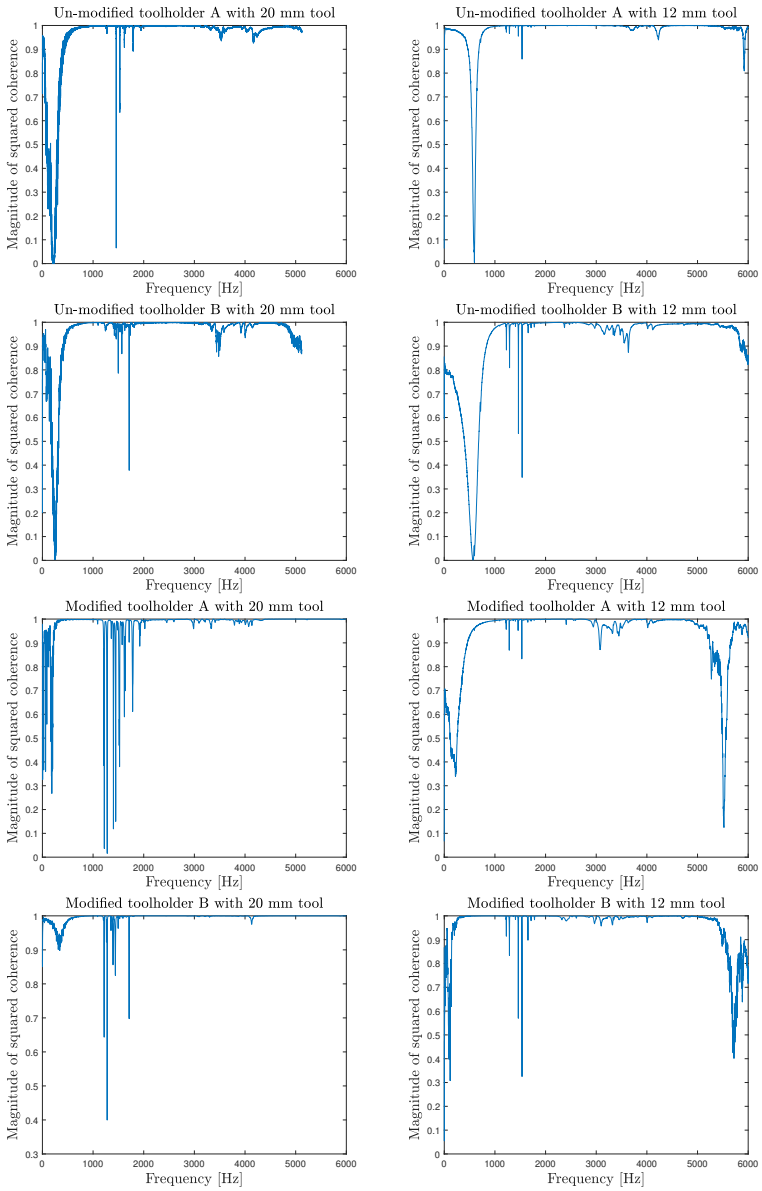

Figure A.1: The coherence for all measurements of dynamics on the tool holders

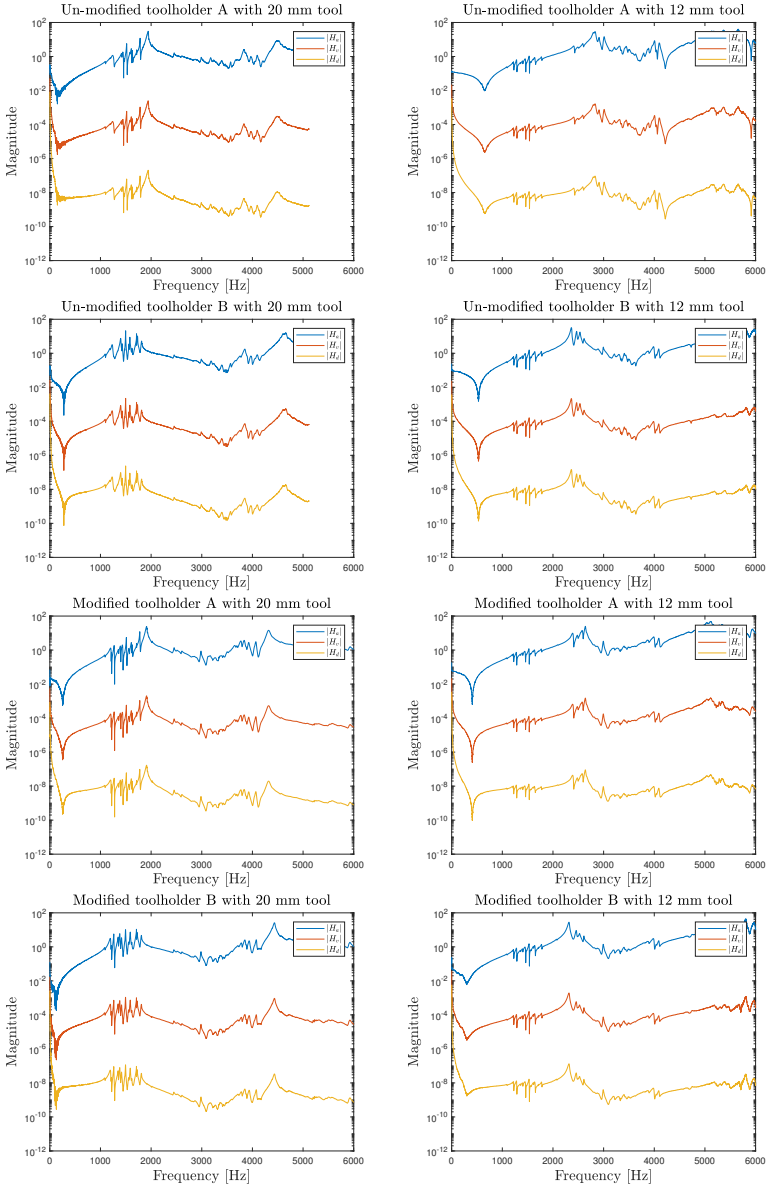

Figure A.2: Transfer functions H_a, H_v, and H_d for all tool holders